PAPER

Partial dynamical symmetries and shape coexistence in nuclei

IOP Publishing | Royal Swedish Academy of Sciences Physica Scripta

Phys. Scr. **92** (2017) 114005 (15pp) https://doi.org/10.1088/1402-4896/aa8697

Partial dynamical symmetries and shape coexistence in nuclei

A Leviatan[1] **and N Gavrielov**

Racah Institute of Physics, The Hebrew University, Jerusalem 91904, Israel

E-mail: ami@phys.huji.ac.il and noam.gavrielov@mail.huji.ac.il

Received 24 May 2017, revised 26 July 2017
Accepted for publication 16 August 2017
Published 25 October 2017

Abstract

We present a symmetry-based approach for shape coexistence in nuclei, founded on the concept of partial dynamical symmetry (PDS). The latter corresponds to the situation where only selected states (or bands of states) of the coexisting configurations preserve the symmetry while other states are mixed. We construct explicitly critical-point Hamiltonians with two or three PDSs of the types U(5), SU(3), $\overline{\mathrm{SU(3)}}$ and SO(6), appropriate to double or triple coexistence of spherical, prolate, oblate and γ-soft deformed shapes, respectively. In each case, we analyze the topology of the energy surface with multiple minima and corresponding normal modes. Characteristic features and symmetry attributes of the quantum spectra and wave functions are discussed. Analytic expressions for quadrupole moments and $E2$ rates involving the remaining solvable states are derived and isomeric states are identified by means of selection rules.

Keywords: dynamical symmetry, partial dynamical symmetry, shape coexistence in nuclei, interacting boson model

(Some figures may appear in colour only in the online journal)

1. Introduction

The presence in the same nuclei, at similar low energies, of two or more sets of states which have distinct properties that can be interpreted in terms of different shapes, is a ubiquitous phenomena across the nuclear chart [1, 2]. The increased availability of rare isotope beams and advancement in high-resolution spectroscopy, open new capabilities to investigate such phenomena in nuclei far from stability [3]. Notable empirical examples include the coexistence of prolate and oblate shapes in the neutron-deficient Kr [4], Se [5] and Hg [6] isotopes and in the neutron-rich Se isotopes [7], the coexistence of spherical and deformed shapes in neutron-rich Sr isotopes [8, 9], ^{96}Zr [10] and near ^{78}Ni [11, 12], and the triple coexistence of spherical, prolate and oblate shapes in ^{186}Pb [13]. A detailed microscopic interpretation of nuclear shape coexistence is a formidable task. In a shell model description of nuclei near shell-closure, it is attributed to the occurrence of multi-particle multi-hole intruder excitations across shell gaps. For medium-heavy nuclei, this necessitates drastic truncations of large model spaces, e.g., by Monte Carlo sampling [14, 15] or by a bosonic approximation of nucleon pairs [16–25]. In a mean-field approach, based on energy density functionals, the coexisting shapes are associated with different minima of an energy surface calculated self-consistently. A detailed comparison with spectroscopic observables requires beyond mean-field methods, including restoration of broken symmetries and configuration mixing of angular momentum and particle-number projected states [26, 27]. Such extensions present a major computational effort and often require simplifying assumptions such as axial symmetry and/or a mapping to collective model Hamiltonians [23–28].

A recent global mean-field calculation of nuclear shape isomers identified experimentally accessible regions of nuclei with multiple minima in their potential-energy surface [29, 30]. Such heavy-mass nuclei awaiting exploration, are beyond the reach of realistic large-scale shell model calculations. With that in mind, we present a simple alternative to describe shape coexistence in medium-heavy nuclei, away from shell-closure, in the framework of the interacting boson model (IBM) [31]. The proposed approach emphasizes the role of remaining underlying symmetries which provide physical insight and make the problem tractable. The

[1] Author to whom any correspondence should be addressed.

feasibility of such a symmetry-based approach gains support from the previously proposed [32, 33] and empirically confirmed [34, 35] analytic descriptions of critical-point nuclei.

2. Dynamical symmetries and nuclear shapes

The IBM has been widely used to describe low-lying quadrupole collective states in nuclei in terms of N monopole ($s^\dagger$) and quadrupole ($d^\dagger$) bosons, representing valence–nucleon pairs. The model has U(6) as a spectrum generating algebra, where the Hamiltonian is expanded in terms of its generators, $\{s^\dagger s,\ s^\dagger d_m,\ d_m^\dagger s,\ d_m^\dagger d_{m'}\}$, and consists of Hermitian, rotational-scalar interactions which conserve the total number of s- and d- bosons, $\hat{N} = \hat{n}_s + \hat{n}_d = s^\dagger s + \sum_m d_m^\dagger d_m$. The solvable limits of the model correspond to DSs associated with chains of nested sub-algebras of U(6), terminating in the invariant SO(3) algebra. A dynamical symmetry (DS) occurs when the Hamiltonian is expressed in terms of the Casimir operators of a given chain,

$$\mathrm{U}(6) \supset \mathrm{G}_1 \supset \mathrm{G}_2 \supset \ \ldots\ \supset \mathrm{SO}(3) \quad |N,\ \lambda_1,\ \lambda_2,\ \ldots,\ L\rangle. \tag{1}$$

In such a case, all states are solvable and classified by quantum numbers, $|N,\ \lambda_1,\ \lambda_2,\ \ldots,\ L\rangle$, which are the labels of irreducible representations (irreps) of the algebras in the chain. Analytic expressions are available for energies and other observables and definite selection rules for transition processes. The DS chains with leading sub-algebras G_1: U(5), SU(3), $\overline{\mathrm{SU(3)}}$ and SO(6), correspond to known paradigms of nuclear collective structure: spherical vibrator, prolate-, oblate- and γ-soft deformed rotors, respectively.

A geometric visualization of the IBM is obtained by an energy surface

$$E_N(\beta,\gamma) = \langle \beta,\gamma;N|\hat{H}|\beta,\gamma;N\rangle, \tag{2}$$

defined by the expectation value of the Hamiltonian in the coherent (intrinsic) state [36, 37],

$$|\beta,\gamma;N\rangle = (N!)^{-1/2}(b_c^\dagger)^N\,|0\,\rangle, \tag{3a}$$

$$b_c^\dagger = (1+\beta^2)^{-1/2}[\beta\cos\gamma d_0^\dagger + \beta\sin\gamma(d_2^\dagger + d_{-2}^\dagger)/\sqrt{2} + s^\dagger]. \tag{3b}$$

Here (β,γ) are quadrupole shape parameters whose values, $(\beta_{\rm eq},\gamma_{\rm eq})$, at the global minimum of $E_N(\beta,\gamma)$ define the equilibrium shape for a given Hamiltonian. The shape can be spherical ($\beta=0$) or deformed ($\beta>0$) with $\gamma=0$ (prolate), $\gamma=\pi/3$ (oblate), $0<\gamma<\pi/3$ (axially asymmetric) or γ-independent. The equilibrium deformations associated with the DS limits conform with their geometric interpretation and are given by $\beta_{\rm eq}=0$ for U(5), $(\beta_{\rm eq}=\sqrt{2},\ \gamma_{\rm eq}=0)$ for SU(3), $(\beta_{\rm eq}=\sqrt{2},\ \gamma_{\rm eq}=\pi/3)$ for $\overline{\mathrm{SU(3)}}$, and $(\beta_{\rm eq}=1,\ \gamma_{\rm eq}$ arbitrary) for SO(6). The DS Hamiltonians support a single minimum in their energy surface, hence serve as benchmarks for the dynamics of a single quadrupole shape (spherical, axially deformed and γ-unstable deformed).

3. Partial dynamical symmetries and multiple nuclear shapes

A DS is characterized by *complete* solvability and good quantum numbers for *all* states. Partial dynamical symmetry (PDS) [38–40] is a generalization of the latter concept, and corresponds to a particular symmetry breaking for which only *some* of the states retain solvability and/or have good quantum numbers. Such generalized forms of symmetries are manifested in nuclear structure, where extensive tests provide empirical evidence for their relevance to a broad range of nuclei [38, 40–57]. In addition to nuclear spectroscopy, Hamiltonians with PDS have been used in the study of quantum phase transitions [58–60] and of systems with mixed regular and chaotic dynamics [61, 62]. In the present work, we show that this novel symmetry notion can play a vital role in formulating algebraic benchmarks for the dynamics of multiple quadrupole shapes.

Coexistence of different shapes involve several states (or bands of states) with distinct properties, reflecting the nature of their dissimilar dynamics. The relevant Hamiltonians, by necessity, contain competing terms with incompatible (non-commuting) symmetries, hence exact dynamical symmetries are broken. In the IBM, the required symmetry breaking is achieved by including in the Hamiltonian terms associated with different DS chains, e.g., by mixing the Casimir operators of the leading sub-algebra in each chain [37]. This mixing and the resulting quantum phase transitions have been studied extensively in the IBM framework [63–68]. In general, under such circumstances, solvability is lost, there are no remaining non-trivial conserved quantum numbers and all eigenstates are expected to be mixed. Shape coexistence near shell-closure was considered within the IBM with configuration mixing, by using different Hamiltonians for the normal and intruder configurations and a number-non-conserving mixing term [16–21]. In the present work, we adapt a different strategy. We construct a single number-conserving Hamiltonian with PDS, which retains the virtues of the relevant dynamical symmetries, but only for selected sets of states associated with each shape. We focus on the dynamics in the vicinity of the critical point where the corresponding multiple minima in the energy surface are near degenerate and the structure changes most rapidly. The construction relies on an intrinsic-collective resolution of the Hamiltonian [69–71], a procedure used formerly in the study of first-order quantum phase transitions [66].

The above indicated resolution amounts to separating the complete Hamiltonian $\hat{H}' = \hat{H} + \hat{H}_c$ into an intrinsic part ($\hat{H}$), which determines the energy surface, and a collective part ($\hat{H}_c$), which is composed of kinetic rotational terms. For a given shape, specified by the equilibrium deformations $(\beta_{\rm eq},\gamma_{\rm eq})$, the intrinsic Hamiltonian is required to annihilate the equilibrium intrinsic state, equation (3),

$$\hat{H}|\beta_{\rm eq},\gamma_{\rm eq};N\rangle = 0. \tag{4}$$

Since the Hamiltonian is rotational-invariant, this condition is equivalent to the requirement that $\hat{H}$ annihilates the states of

good angular momentum L projected from $|\beta_{\rm eq}, \gamma_{\rm eq}; N\rangle$

$$\hat{H}|\beta_{\rm eq}, \gamma_{\rm eq}; N, x, L\rangle = 0. \quad (5)$$

Here x denotes additional quantum numbers needed to characterize the states and, for simplicity, we have omitted the irrep label M of SO(2) $\subset$ SO(3). Symmetry considerations enter when $(\beta_{\rm eq}, \gamma_{\rm eq})$ coincide with the equilibrium deformations of the DS chains, mentioned in section 2. In this case, the equilibrium intrinsic state, $|\beta_{\rm eq}, \gamma_{\rm eq}; N\rangle$, becomes a lowest (or highest) weight state in a particular irrep, $\lambda_{\rm I} = \Lambda_0$, of the leading sub-algebra G_1 in the chain of equation (1). The projected states, $|\beta_{\rm eq}, \gamma_{\rm eq}; N, \lambda_{\rm I} = \Lambda_0, \lambda_2, \ldots, L\rangle$, are now specified by the quantum numbers of the algebras in the chain and the intrinsic Hamiltonian $\hat{H}$ satisfies

$$\hat{H}|\beta_{\rm eq}, \gamma_{\rm eq}; N, \lambda_{\rm I} = \Lambda_0, \lambda_2, \ldots, L\rangle = 0. \quad (6)$$

The set of zero-energy eigenstates in equation (6) are basis states of the particular G_1-irrep, $\lambda_{\rm I} = \Lambda_0$, and have good G_1 symmetry. For a positive-definite $\hat{H}$, they span the ground band of the equilibrium shape. $\hat{H}$ itself, however, need not be invariant under G_1 and, therefore, has partial-G_1 symmetry. Identifying the collective part with the Casimir operators of the remaining sub-algebras of G_1 in the chain (1), the degeneracy of the above set of states is lifted, and they remain solvable eigenstates of the complete Hamiltonian. The latter, by definition, has G_1-PDS. According to the PDS algorithms [39, 49], the construction of number-conserving Hamiltonians obeying the condition of equation (6), is facilitated by writing them in normal-order form, $\hat{H} = \sum_{\alpha,\beta} u_{\alpha\beta} \hat{T}^{\dagger}_{\alpha} \hat{T}_{\beta}$, in terms of n-particle creation and annihilation operators satisfying

$$\hat{T}_{\alpha}|\beta_{\rm eq}, \gamma_{\rm eq}; N, \lambda_{\rm I} = \Lambda_0, \lambda_2, \ldots, L\rangle = 0. \quad (7)$$

A large number of purely bosonic [38–41, 46, 48–50], purely fermionic [51, 52] and Bose–Fermi [57] Hamiltonians with PDS have been constructed in this manner. With a few exceptions [58–60], they all involved a single PDS. We now wish to extend the above procedure to encompass a construction of Hamiltonians with several distinct PDSs, relevant to coexistence of multiple shapes. For that purpose, consider two different shapes specified by equilibrium deformations (β_1, γ_1) and (β_2, γ_2) whose dynamics is described, respectively, by the following DS chains:

$$\mathrm{U(6)} \supset \mathrm{G_1} \supset \mathrm{G_2} \supset \ldots \supset \mathrm{SO(3)} \quad |N, \lambda_1, \lambda_2, \ldots, L\rangle, \quad (8a)$$

$$\mathrm{U(6)} \supset \mathrm{G_1'} \supset \mathrm{G_2'} \supset \ldots \supset \mathrm{SO(3)} \quad |N, \sigma_1, \sigma_2, \ldots, L\rangle, \quad (8b)$$

with different leading sub-algebras ($G_1 \neq G_1'$) and associated bases. At the critical point, the corresponding minima representing the two shapes and the respective ground bands are degenerate. Accordingly, we require the intrinsic critical-point Hamiltonian to satisfy simultaneously the following two conditions:

$$\hat{H}|\beta_1, \gamma_1; N, \lambda_{\rm I} = \Lambda_0, \lambda_2, \ldots, L\rangle = 0, \quad (9a)$$

$$\hat{H}|\beta_2, \gamma_2; N, \sigma_1 = \Sigma_0, \sigma_2, \ldots, L\rangle = 0. \quad (9b)$$

The states of equation (9*a*) reside in the $\lambda_{\rm I} = \Lambda_0$ irrep of G_1, are classified according to the DS chain (8*a*), hence have good G_1 symmetry. Similarly, the states of equation (9*b*) reside in the $\sigma_1 = \Sigma_0$ irrep of G_1', are classified according to the DS chain (8*b*), hence have good G_1' symmetry. Although G_1 and G_1' are incompatible, both sets are eigenstates of the same Hamiltonian. When the latter is positive definite, the two sets span the ground bands of the (β_1, γ_1) and (β_2, γ_2) shapes, respectively. In general, $\hat{H}$ itself is not necessarily invariant under G_1 nor under G_1' and, therefore, its other eigenstates can be mixed under both G_1 and G_1'. Identifying the collective part of the Hamiltonian with the Casimir operator of SO(3) (as well as with the Casimir operators of additional algebras which are common to both chains), the two sets of states remain (non-degenerate) eigenstates of the complete Hamiltonian which then has both G_1-PDS and G_1'-PDS. The case of triple (or multiple) shape coexistence, associated with three (or more) incompatible DS chains is treated in a similar fashion. In the following sections, we apply this procedure to a variety of coexisting shapes, examine the spectral properties of the derived PDS Hamiltonians, and highlight their potential to serve as benchmarks for describing multiple shapes in nuclei.

4. Spherical and axially-deformed shape coexistence: U(5)-SU(3) PDS

A particular type of shape coexistence present in nuclei, involves spherical and axially deformed shapes. The relevant DS chains for such configurations are [31],

$$\mathrm{U(6)} \supset \mathrm{U(5)} \supset \mathrm{SO(5)} \supset \mathrm{SO(3)} \quad |N, n_d, \tau, n_\Delta, L\rangle, \quad (10a)$$

$$\mathrm{U(6)} \supset \mathrm{SU(3)} \supset \mathrm{SO(3)} \quad |N, (\lambda, \mu), K, L\rangle. \quad (10b)$$

The U(5)-DS limit of equation (10*a*) is appropriate to the dynamics of a spherical shape. For a given U(6) irrep N, the allowed U(5) and SO(5) irreps are $n_d = 0, 1, 2, \ldots, N$ and $\tau = n_d, n_d - 2, \ldots 0$ or 1, respectively. The values of L contained in a given τ-irrep follow the SO(5) $\supset$ SO(3) reduction rules [31] and n_Δ is a multiplicity label. The basis states, $|N, n_d, \tau, n_\Delta, L\rangle$, are eigenstates of the Casimir operators $\hat{C}_1[\mathrm{U(5)}] = \hat{n}_d$, $\hat{C}_2[\mathrm{U(5)}] = \hat{n}_d(\hat{n}_d + 4)$, $\hat{C}_2[\mathrm{SO(5)}] = 2\sum_{\ell=1,3} U^{(\ell)} \cdot U^{(\ell)}$ and $\hat{C}_2[\mathrm{SO(3)}] = L^{(1)} \cdot L^{(1)}$, with eigenvalues n_d, $n_d(n_d + 4)$, $\tau(\tau + 3)$ and $L(L + 1)$, respectively. Here $\hat{C}_k[\mathrm{G}]$ denotes the Casimir operator of G of order k, $\hat{n}_d = \sqrt{5}\, U^{(0)}$, $L^{(1)} = \sqrt{10}\; U^{(1)}$, with $U^{(\ell)} = (d^{\dagger}\tilde{d})^{(\ell)}$, $\tilde{d}_m = (-1)^m d_{-m}$ and standard notation of angular momentum coupling is used. The U(5)-DS Hamiltonian involves a linear combination of these Casimir operators. The spectrum resembles that of an anharmonic spherical vibrator, describing quadrupole excitations of a spherical shape. The splitting of states in a given U(5) n_d-multiplet is governed by the SO(5) and SO(3) terms. The lowest U(5) multiplets involve the ground state with quantum numbers ($n_d = 0$, $\tau = 0$, $L = 0$) and excited states with quantum numbers ($n_d = 1$, $\tau = 1$, $L = 2$),

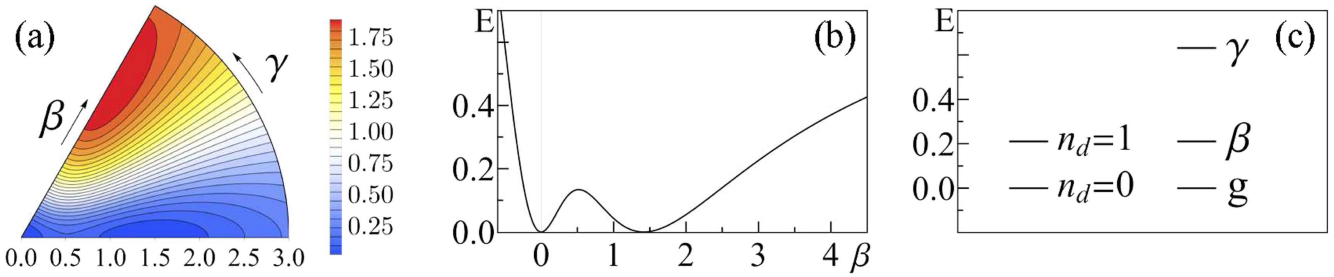

Figure 1. Spherical-prolate (S-P) shape coexistence. (a) Contour plots of the energy surface (17), (b) $\gamma = 0$ sections, and (c) bandhead spectrum, for the Hamiltonian $\hat{H}'$ (22) with parameters $h_2 = 1$, $\rho = 0$ and $N = 20$.

($n_d = 2$, $\tau = 0$, $L = 0$; $\tau = 2$, $L = 2, 4$) and ($n_d = 3$, $\tau = 3$, $L = 6, 4, 3, 0$; $\tau = 1$, $L = 2$).

The SU(3)-DS limit of equation (10*b*) is appropriate to the dynamics of a prolate-deformed shape. For a given N, the allowed SU(3) irreps are $(\lambda, \mu) = (2N - 4k - 6m, 2k)$ with k, m, non-negative integers. The values of L contained in a given (λ, μ)-irrep follow the SU(3) $\supset$ SO(3) reduction rules [31] and the multiplicity label K corresponds geometrically to the projection of the angular momentum on the symmetry axis. The basis states are eigenstates of the Casimir operator $\hat{C}_2[SU(3)] = 2Q^{(2)} \cdot Q^{(2)} + \frac{3}{4}L^{(1)} \cdot L^{(1)}$ with eigenvalues $\lambda(\lambda + 3) + \mu(\mu + 3) + \lambda\mu$. The generators of SU(3) are the angular momentum operators $L^{(1)}$ defined above, and the quadrupole operators

$$Q^{(2)} = d^\dagger s \quad + \quad s^\dagger \tilde{d} - \frac{1}{2}\sqrt{7}\,(d^\dagger \tilde{d})^{(2)}. \tag{11}$$

The SU(3)-DS Hamiltonian involves a linear combination of $\hat{C}_2[SU(3)]$ and $\hat{C}_2[SO(3)]$, and its spectrum resembles that of an axially deformed rotovibrator composed of SU(3) (λ, μ)-multiplets forming rotational bands with $L(L + 1)$-splitting. The lowest irrep $(2N, 0)$ contains the ground band $g(K = 0)$ of a prolate-deformed nucleus. The first excited irrep $(2N - 4, 2)$ contains both the $\beta(K = 0)$ and $\gamma(K = 2)$ bands.

In discussing properties of the SU(3)-DS spectrum, it is convenient to subtract from $\hat{C}_2[\mathrm{SU}(3)]$ the ground-state energy, and consider the following positive-definite term:

$$\hat{\theta}_2 \equiv -\hat{C}_2[\mathrm{SU}(3)] + 2\hat{N}(2\hat{N} + 3) = P_0^\dagger P_0 + P_2^\dagger \cdot \tilde{P}_2, \tag{12}$$

where $\tilde{P}_{2m} = (-)^m P_{2,-m}$. The SU(3) basis states, $|N, (\lambda, \mu), K, L\rangle$, are eigenstates of $\hat{\theta}_2$ with eigenvalues $(2N - \lambda)(2N + \lambda + 3) - \mu(\lambda + \mu + 3)$ and the ground band with $(\lambda, \mu) = (2N, 0)$ occurs at zero energy. The two-boson pair operators

$$P_0^\dagger = d^\dagger \cdot d^\dagger - 2(s^\dagger)^2, \tag{13a}$$

$$P_{2m}^\dagger = 2d_m^\dagger s^\dagger + \sqrt{7}\,(d^\dagger\, d^\dagger)_m^{(2)}, \tag{13b}$$

are (0, 2) tensors with respect to SU(3) and satisfy

$$P_0\,|N, (\lambda, \mu) = (2N, 0), K = 0, L\rangle = 0,$$
$$P_{2m}\,|N, (\lambda, \mu) = (2N, 0), K = 0, L\rangle = 0. \tag{14}$$

These operators correspond to $\hat{T}_\alpha$ of equation (7) and, as shown below, they play a central role in the construction of Hamiltonians with SU(3)-PDS.

Considering the case of coexisting spherical and prolate-deformed shapes, following the procedure outlined in equation (9), the intrinsic part of the critical-point Hamiltonian is required to satisfy

$$\hat{H}|N, (\lambda, \mu) = (2N, 0), K = 0, L\rangle = 0$$
$$L = 0, 2, 4, \ldots, 2N \tag{15a}$$

$$\hat{H}|N, n_d = 0, \tau = 0, L = 0\rangle = 0. \tag{15b}$$

Equivalently, $\hat{H}$ annihilates both the intrinsic state of equation (3) with $(\beta = \sqrt{2}, \gamma = 0)$, which is the lowest weight vector in the SU(3) irrep $(\lambda, \mu) = (2N, 0)$, and the intrinsic state with $\beta = 0$, which is the single basis state in the U(5) irrep $n_d = 0$. The resulting intrinsic critical-point Hamiltonian is found to be [58],

$$\hat{H} = h_2\, P_2^\dagger \cdot \tilde{P}_2, \tag{16}$$

where $P_{2m}^\dagger$ is given in equation (13*b*). The corresponding energy surface, $E_N(\beta, \gamma) = N(N - 1)\tilde{E}(\beta, \gamma)$, is given by

$$\tilde{E}(\beta, \gamma) = 2h_2\beta^2\,(\,\beta^2 - 2\sqrt{2}\,\beta\cos 3\gamma + 2\,)(1 + \beta^2)^{-2}. \tag{17}$$

The surface is linear in $\Gamma = \cos 3\gamma$, at most quartic in β, and can be transcribed as $\tilde{E}(\beta, \gamma) = (1 + \beta^2)^{-2}(a\beta^2 - b\beta^3\Gamma + c\beta^4)$, with $b^2 = 4ac$ and $a = 4h_2$, $b = 4\sqrt{2}\,h_2$, $c = 2h_2$. It is the most general form of a surface accommodating degenerate spherical and axially-deformed extrema, for an Hamiltonian with one- and two-body terms. For $h_2 > 0$, $\hat{H}$ is positive definite and $\tilde{E}(\beta, \gamma)$ has two degenerate global minima, $\beta = 0$ and $(\beta = \sqrt{2}, \gamma = 0)$, at $\tilde{E} = 0$. Additional extremal points include (i) a saddle point: $[\beta = \beta_* = (\sqrt{3} - 1)/\sqrt{2}, \gamma = 0]$, which supports a barrier of height $\tilde{E}_{\mathrm{bar}} = \frac{1}{2}h_2(\sqrt{3} - 1)^2 = 0.268h_2$, and (ii) a local maximum: $[\beta = \beta_{**} = (\sqrt{3} + 1)/\sqrt{2}, \gamma = \pi/3]$ [or equivalently $(\beta = -\beta_{**}, \gamma = 0)$], at $\tilde{E}_{\max} = \frac{1}{2}h_2(\sqrt{3} + 1)^2$. Figures 1(a) and (b) show the energy surface contour, $\tilde{E}(\beta, \gamma)$, and section, $\tilde{E}(\beta, \gamma = 0)$, of $\hat{H}$, respectively. The barrier separating the two minima satisfies $\tilde{E}_{\mathrm{bar}} = 0.13\tilde{E}_{\mathrm{lim}}$, where $\tilde{E}_{\mathrm{lim}} = \tilde{E}(\beta \to \infty, \gamma) = 2h_2$. It is significantly higher than typical barriers of order $0.001\tilde{E}_{\mathrm{lim}}$,

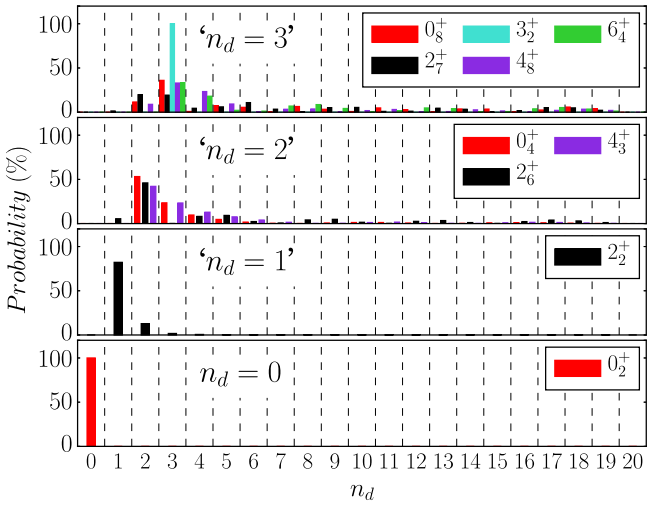

Figure 2. U(5) n_d-decomposition for spherical states, eigenstates of the Hamiltonian $\hat{H}'$ (22) with parameters as in figure 1, resulting in spherical-prolate shape coexistence.

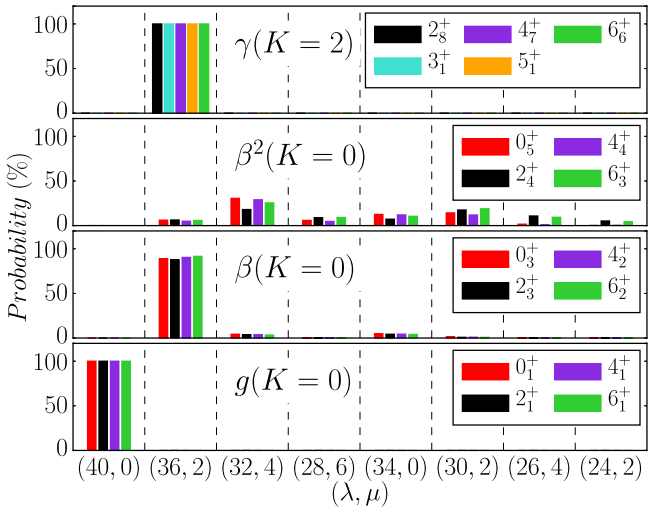

Figure 3. SU(3) (λ, μ)-decomposition for members of the prolate-deformed g, β, β^2 and γ bands, eigenstates of the Hamiltonian $\hat{H}'$ (22) with parameters as in figure 1. Shown are probabilities larger than 4%.

obtained in standard Hamiltonians mixing the U(5) and SU(3) Casimir operators [65]. The normal modes of the Hamiltonian (16) correspond to small oscillations about the respective minima of its energy surface. For large N, the deformed normal modes involve one-dimensional β vibration and two-dimensional γ vibrations about the prolate-deformed global minimum, with frequencies

$$\epsilon_\beta = 4h_2 N, \tag{18a}$$

$$\epsilon_\gamma = 12h_2 N. \tag{18b}$$

The spherical normal modes involve five-dimensional quadrupole vibrations about the spherical global minimum, with frequency

$$\epsilon = 4h_2 N. \tag{19}$$

The bandhead spectrum associated with these modes, is shown in figure 1(c). Interestingly, the spherical and β modes have the same energy and are considerably lower than the γ mode, $\epsilon = \epsilon_\beta = \epsilon_\gamma/3$. This is consistent with the observed enhanced density of low-lying 0^+ states, signaling the transitional region of such a first-order quantum phase transition [72, 73].

By construction, the members of the prolate-deformed ground band $g(K = 0)$, equation (15*a*), have good SU(3) quantum numbers $(\lambda, \mu) = (2N, 0)$, and the spherical ground state, equation (15*b*), has good U(5) quantum numbers $(n_d = \tau = L = 0)$. The Hamiltonian $\hat{H}$ of equation (16) has additional solvable SU(3) basis states with $(\lambda, \mu) = (2N - 4k, 2k)K = 2k$, which span the deformed $\gamma^k(K = 2k)$ bands, and an additional solvable U(5) basis state with $n_d = \tau = L = 3$. Altogether, although $\hat{H}$ is neither SU(3)-invariant nor U(5)-invariant, it has a subset of solvable states with good SU(3) symmetry

$$|N, (2N, 0)K = 0, L\rangle \qquad E = 0$$
$$L = 0, 2, 4, \ldots, 2N, \tag{20a}$$

$$|N, (2N - 4k, 2k)K = 2k, L\rangle \; E = h_2\, 6k(2N - 2k + 1)$$
$$L = K, K + 1, \ldots, (2N - 2k), \tag{20b}$$

and, simultaneously, a subset of solvable states with good U(5) symmetry

$$|N, n_d = \tau = L = 0\rangle \qquad E = 0, \tag{21a}$$

$$|N, n_d = \tau = L = 3\rangle \qquad E = 6(2N - 1). \tag{21b}$$

The spherical $L = 0$ state, equation (21*a*), is degenerate with the prolate-deformed ground band, equation (20*a*), and the spherical $L = 3$ state, equation (21*b*), is degenerate with the γ band, equation (20*b*) with $k = 1$. Identifying the collective part with $\hat{C}_2[\mathrm{SO}(3)]$, we arrive at the following complete Hamiltonian

$$\hat{H}' = h_2\, P_2^\dagger \cdot \tilde{P}_2 + \rho\, \hat{C}_2[\mathrm{SO}(3)]. \tag{22}$$

The added rotational term generates an exact $L(L + 1)$ splitting without affecting the wave functions. In particular, the solvable subsets of eigenstates, equations (20) and (21), remain intact. Other eigenstates, as shown below, can mix strongly with respect to both SU(3) and U(5).

The symmetry structure of the Hamiltonian eigenstates can be inferred from the probability distributions, $P^{(N,L)}_{n_d} = \sum_{\tau,n_\Delta} |C^{(N,L)}_{n_d,\tau,n_\Delta}|^2$ and $P^{(N,L)}_{(\lambda,\mu)} = \sum_K |C^{(N,L)}_{(\lambda,\mu),K}|^2$, obtained from their expansion coefficients in the U(5) and SU(3) bases (10), respectively. In general, the low-lying spectrum of $\hat{H}'$ (22) exhibits two distinct type of states, spherical and deformed. Spherical type of states show a narrow n_d-distribution, with a characteristic dominance of a single n_d component. Figure 2 shows the U(5) n_d-decomposition of such states, selected on the basis of having the largest components with $n_d = 0, 1, 2, 3$, within the given L spectra. States with different L values are arranged into panels labeled 'n_d' to conform with the structure of the n_d-multiplets of a spherical vibrator. The lowest spherical $L = 0_2^+$ state is seen to be a

pure $n_d = 0$ state which is the solvable U(5) state of equation (21*a*). The $L = 2_2^+$ state has a pronounced $n_d = 1$ component ($\sim 80\%$), whose origin can be traced to the relation

$$\hat{H}|N, n_d = \tau = 1, L = 2\rangle = h_2\, 4(N-1)\Big[|N, n_d = \tau = 1, L = 2\rangle + \sqrt{\tfrac{7}{2(N-1)}}\,|N, n_d = \tau = L = 2\rangle\Big]. \quad (23)$$

As seen, the U(5)-basis state $|N, n_d = \tau = 1, L = 2\rangle$ approaches the status of an eigenstate for large N, with corrections of order $1/\sqrt{N}$. The states ($L = 0_4^+, 2_6^+, 4_3^+$) in the third panel of figure 2, have a less pronounced ($\sim 50\%$) single $n_d = 2$ component. The higher-energy states in the panel '$n_d = 3$' are significantly fragmented, with a notable exception of $L = 3_2^+$, which is the solvable U(5) basis state of equation (21*b*).

The deformed type of states have a different character. They exhibit a broad n_d-distribution, as seen clearly in the following expansion of the SU(3) ground band wave functions in the U(5) basis:

$$|N, (2N, 0)K = 0, L\rangle = \sum_{n_d,\tau,n_\Delta} \frac{1}{2}[1 + (-1)^{n_d-\tau}] \times \xi^{(N,L)}_{n_d,\tau,n_\Delta}|N, n_d, \tau, n_\Delta, L\rangle, \quad (24a)$$

$$\xi^{(N,L)}_{n_d,\tau,n_\Delta} = \left[\frac{N!(2N-L)!!(2N+L+1)!!}{3^N(2N)!(N-n_d)!(n_d-\tau)!!(n_d+\tau+3)!!}\right]^{1/2} \times (\sqrt{2})^{n_d} f^{(L)}_{\tau,n_\Delta}. \quad (24b)$$

Explicit expressions of $f^{(L)}_{\tau,n_\Delta}$ for $L = 0, 2, 4$ are documented in [38]. The U(5) n_d-probability inferred from equation (24), shows that the contribution of each individual n_d-component is exponentially small for large N. Figure 3 shows the SU(3) (λ, μ)-distribution for such deformed type of states, members of the $g(K = 0)$, $\beta(K = 0)$, $\beta^2(K = 0)$ and $\gamma(K = 2)$ bands. The ground $g(K = 0)$ and $\gamma(K = 2)$ bands are pure with $(\lambda, \mu) = (2N, 0)$ and $(2N - 4, 2)$ SU(3) character, respectively. These are the solvable bands of equation (20) with good SU(3) quantum numbers. The non-solvable K-bands, e.g. the $\beta(K = 0)$ and $\beta^2(K = 0)$ in figure 3, show considerable SU(3) mixing, and the mixing is coherent, i.e., similar for different L-states in the same band. The above analysis demonstrates that some eigenstates of the critical-point Hamiltonian (22) have good U(5) symmetry (either exactly or to a good approximation for large N), some eigenstates have good SU(3) symmetry, and all other states are mixed with respect to both U(5) and SU(3). This defines U(5)-PDS coexisting with SU(3)-PDS. These persisting competing symmetries affect the dynamics at the critical point, which has a mixed regular and chaotic character [59].

Since the wave functions for the solvable states, equations (20) and (21), are known, one has at hand closed form expressions for electromagnetic moments and rates. Taking the $E2$ operator to be proportional to the SU(3) quadrupole operator of equation (11) with an effective charge e_B, $T(E2) = e_B\, Q^{(2)}$, the $B(E2)$ values for intraband ($g \to g$) transitions between states of the ground band (20*a*) and quadrupole moments are given by the known SU(3)-DS expressions [31]

$$Q_L = -e_B\sqrt{\tfrac{16\pi}{40}}\,\tfrac{L}{2L+3}(4N+3), \quad (25a)$$

$$B(E2; g, L+2 \to g, L) = e_B^2\,\tfrac{3(L+1)(L+2)}{4(2L+3)(2L+5)}\,(2N-L)(2N+L+3). \quad (25b)$$

Similarly, the quadrupole moment of the solvable spherical $L = 3$ state of equation (21*b*), obeys the U(5)-DS expression

$$Q_{L=3} = -e_B 3\sqrt{\tfrac{16\pi}{40}}. \quad (26)$$

The spherical states, equation (21), are not connected by $E2$ transitions to states of the ground band (20*a*), since the latter exhaust the $(2N, 0)$ irrep of SU(3) and $Q^{(2)}$, as a generator, cannot connect different (λ, μ)-irreps of SU(3). As will be discussed in section 6, weak spherical → deformed $E2$ transitions persist also for a more general $E2$ operator, obtained by adding to $T(E2)$ the term $d^\dagger s + s^\dagger\tilde{d}$. The latter, however, can connect by $E2$ transitions the ground with excited β and γ bands. Since both the $g(K = 0)$ and $\gamma(K = 2)$ bands are solvable with good SU(3) symmetry, equation (20), analytic expressions for $\gamma \to g$ $E2$ rates are available [40, 74]. There are also no $E0$ transitions involving the spherical states (21), since the $E0$ operator $T(E0) \propto \hat{n}_d$, is diagonal in n_d.

The above discussion has focused on the dynamics in the vicinity of the critical point where the spherical and deformed minima are near degenerate. The evolution of structure away from the critical point can be studied by incorporating additional terms into $\hat{H}'$ (22). Adding an $\epsilon\hat{n}_d$ term, will leave the solvable spherical states (21) unchanged, but will shift the deformed ground band to higher energy of order $2\epsilon N/3$. Similarly, adding a small $\alpha\hat{\theta}_2$ term, equation (12), will leave the solvable SU(3) bands unchanged but will shift the spherical ground state ($n_d = L = 0$) to higher energy of order $4\alpha N^2$. The selection rules discussed above, ensure that the $L = 0$ state of the excited configuration will have significantly retarded $E2$ and $E0$ decays to states of the lower configuration, hence will have the attributes of an isomer state.

5. Prolate-oblate shape coexistence: SU(3)-$\overline{SU(3)}$ PDS

Shape coexistence in nuclei can involve two deformed shapes, i.e., prolate and oblate. The relevant DS limits for the latter configurations are [31],

$$\mathrm{U(6)} \supset \mathrm{SU(3)} \supset \mathrm{SO(3)} \qquad |N, (\lambda, \mu), K, L\rangle, \quad (27a)$$

$$\mathrm{U(6)} \supset \overline{\mathrm{SU(3)}} \supset \mathrm{SO(3)} \qquad |N, (\bar{\lambda}, \bar{\mu}), \bar{K}, L\rangle. \quad (27b)$$

The SU(3)-DS chain (27*a*), appropriate to a prolate shape, was discussed in section 4. The $\overline{\mathrm{SU(3)}}$-DS chain (27*b*), appropriate to an oblate shape, has similar properties but now the allowed $\overline{\mathrm{SU(3)}}$ irreps are $(\bar{\lambda}, \bar{\mu}) = (2k, 2N - 4k - 6m)$ with k, m, non-negative integers, and the multiplicity label is denoted by $\bar{K}$. The basis states are eigenstates of the Casimir

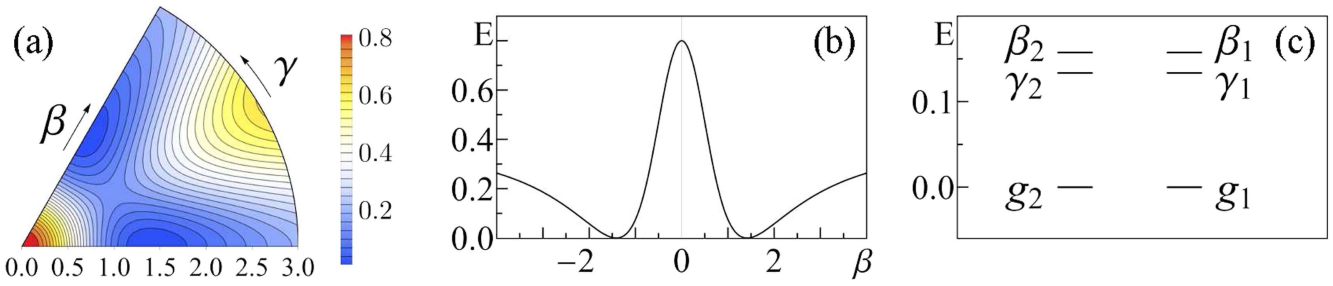

Figure 4. Prolate-oblate (P-O) shape coexistence. (a) Contour plots of the energy surface (31), (b) $\gamma = 0$ sections, and (c) bandhead spectrum, for the Hamiltonian $\hat{H}'$ (33) with parameters $h_0 = 0.2$, $h_2 = 0.4$, $\eta_3 = 0.567$, $\alpha = 0.018$, $\rho = 0$ and $N = 20$.

operator $\hat{C}_2[\overline{\mathrm{SU(3)}}] = 2\bar{Q}^{(2)} \cdot \bar{Q}^{(2)} + \frac{3}{4}L^{(1)} \cdot L^{(1)}$, with eigenvalues $\bar{\lambda}(\bar{\lambda}+3) + \bar{\mu}(\bar{\mu}+3) + \bar{\lambda}\bar{\mu}$. Here $\bar{Q}^{(2)}$ are the quadrupole operators given by

$$\bar{Q}^{(2)} = d^\dagger s \quad + \quad s^\dagger \tilde{d} + \frac{1}{2}\sqrt{7}\,(d^\dagger \tilde{d})^{(2)}, \tag{28}$$

and $L^{(1)}$ are the angular momentum operators. The generators of SU(3) and $\overline{\mathrm{SU(3)}}$, $Q^{(2)}$ (11) and $\bar{Q}^{(2)}$ (28), and corresponding basis states, $|N, (\lambda, \mu), K, L\rangle$ and $|N, (\bar{\lambda}, \bar{\mu}), \bar{K}, L\rangle$, are related by a change of phase $(s^\dagger, s) \rightarrow (-s^\dagger, -s)$, induced by the operator $\mathcal{R}_s = \exp(i\pi\hat{n}_s)$, with $\hat{n}_s = s^\dagger s$. As previously mentioned, in the SU(3)-DS, the prolate ground band $g(K=0)$ has $(2N, 0)$ character and the $\beta(K=0)$ and $\gamma(K=2)$ bands have $(2N-4, 2)$. In the $\overline{\mathrm{SU(3)}}$-DS, the oblate ground band $g(\bar{K}=0)$ has $(0, 2N)$ character and the excited $\beta(\bar{K}=0)$ and $\gamma(\bar{K}=2)$ bands have $(2, 2N-4)$. Henceforth, we denote such prolate and oblate bands by (g_1, β_1, γ_1) and (g_2, β_2, γ_2), respectively. Since $\mathcal{R}_s Q^{(2)} \mathcal{R}_s^{-1} = -\bar{Q}^{(2)}$, the SU(3) and $\overline{\mathrm{SU(3)}}$ DS spectra are identical and the quadrupole moments of corresponding states differ in sign.

The phase transition between prolate and oblate shapes has been previously studied by varying a control parameter in the IBM Hamiltonian [75, 76]. The latter, however, consisted of one- and two-body terms hence could not accommodate simultaneously two deformed minima. For that reason, in the present approach, we consider an Hamiltonian with cubic terms which retains the virtues of SU(3) and $\overline{\mathrm{SU(3)}}$ DSs for the prolate and oblate ground bands. Following the procedure of equation (9), the intrinsic part of such critical-point Hamiltonian is required to satisfy

$$\hat{H}|N, (\lambda, \mu) = (2N, 0), K = 0, L\rangle = 0, \tag{29a}$$

$$\hat{H}|N, (\bar{\lambda}, \bar{\mu}) = (0, 2N), \bar{K} = 0, L\rangle = 0. \tag{29b}$$

Equivalently, $\hat{H}$ annihilates the intrinsic states of equation (3), with $(\beta = \sqrt{2}, \gamma = 0)$ and $(\beta = -\sqrt{2}, \gamma = 0)$, which are the lowest- and highest-weight vectors in the irreps $(2N, 0)$ and $(0, 2N)$ of SU(3) and $\overline{\mathrm{SU(3)}}$, respectively. The resulting Hamiltonian is found to be [60],

$$\hat{H} = h_0\, P_0^\dagger \hat{n}_s P_0 + h_2\, P_0^\dagger \hat{n}_d P_0 + \eta_3\, G_3^\dagger \cdot \tilde{G}_3, \tag{30}$$

where $P_0^\dagger$ is given in equation (13*a*), $G_{3,\mu}^\dagger = \sqrt{7}\,[(d^\dagger d^\dagger)^{(2)} d^\dagger]_\mu^{(3)}$, $\tilde{G}_{3,\mu} = (-1)^\mu G_{3,-\mu}$. The corresponding energy surface, $E_N(\beta, \gamma) = N(N-1)(N-2)\tilde{E}(\beta, \gamma)$, is given by

$$\tilde{E}(\beta, \gamma) = \{(\beta^2 - 2)^2[h_0 + h_2\beta^2] + \eta_3\beta^6 \sin^2(3\gamma)\}(1+\beta^2)^{-3}. \tag{31}$$

The surface is an even function of β and $\Gamma = \cos 3\gamma$, and can be transcribed as $\tilde{E}(\beta, \gamma) = z_0 + (1+\beta^2)^{-3}\,[A\beta^6 + B\beta^6\Gamma^2 + D\beta^4 + F\beta^2]$, with $A = -4h_0 + h_2 + \eta_3$, $B = -\eta_3$, $D = -(11h_0 + 4h_2)$, $F = 4(h_2 - 4h_0)$, $z_0 = 4h_0$. It is the most general form of a surface accommodating degenerate prolate and oblate extrema with equal β-deformations, for an Hamiltonian with cubic terms [77, 78]. For $h_0, h_2, \eta_3 \geqslant 0$, $\hat{H}$ is positive definite and $\tilde{E}(\beta, \gamma)$ has two degenerate global minima, $(\beta = \sqrt{2}, \gamma = 0)$ and $(\beta = \sqrt{2}, \gamma = \pi/3)$ [or equivalently $(\beta = -\sqrt{2}, \gamma = 0)$], at $\tilde{E} = 0$. $\beta = 0$ is always an extremum, which is a local minimum (maximum) for $F > 0$ $(F < 0)$, at $\tilde{E} = 4h_0$. Additional extremal points include (i) a saddle point: $[\beta_*^2 = \frac{2(4h_0 - h_2)}{h_0 - 7h_2}, \gamma = 0, \pi/3]$, at $\tilde{E} = \frac{4(h_0 + 2h_2)^3}{81(h_0 - h_2)^2}$. (ii) A local maximum and a saddle point: $[\beta_{**}^2, \gamma = \pi/6]$, at $\tilde{E} = \frac{1}{3}(1+\beta_{**}^2)^{-2}\ \beta_{**}^2[D\beta_{**}^2 + 2F] + z_0$, where β_{**}^2 is a solution of $(D-3A)\beta_{**}^4 \ + \ 2(F-D)\beta_{**}^2 - F = 0$. The saddle points, when they exist, support a barrier separating the various minima, as seen in figure 4. For large N, the normal modes involve β and γ vibrations about the respective deformed minima, with frequencies

$$\epsilon_{\beta 1} = \epsilon_{\beta 2} = \frac{8}{3}(h_0 + 2h_2)N^2, \tag{32a}$$

$$\epsilon_{\gamma 1} = \epsilon_{\gamma 2} = 4\eta_3 N^2. \tag{32b}$$

Figures 4(a)–(c) show $\tilde{E}(\beta, \gamma)$, $\tilde{E}(\beta, \gamma = 0)$ and the bandhead spectrum, respectively, with parameters ensuring P-O global minima and a local maximum at $\beta = 0$.

The members of the prolate and oblate ground bands, equation (29), are zero-energy eigenstates of $\hat{H}$ (30), with good SU(3) and $\overline{\mathrm{SU(3)}}$ symmetry, respectively. The Hamiltonian is invariant under a change of sign of the s-bosons, hence commutes with the $\mathcal{R}_s$ operator mentioned above. Consequently, all non-degenerate eigenstates of $\hat{H}$ have well-defined s-parity. This implies vanishing quadrupole moments for an $E2$ operator which is odd under such sign change. To overcome this difficulty, we introduce a small s-parity breaking term $\alpha\hat{\theta}_2$, equation (12), which contributes to $\tilde{E}(\beta, \gamma)$ a component $\tilde{\alpha}(1+\beta^2)^{-2}\ \ [(\beta^2-2)^2 + 2\beta^2(2 - 2\sqrt{2}\,\beta\Gamma + \beta^2)]$, with $\tilde{\alpha} = \alpha/(N-2)$. The linear Γ-dependence distinguishes the two deformed minima and slightly lifts their degeneracy, as well as that of the normal modes (32). Replacing $\hat{\theta}_2$ by

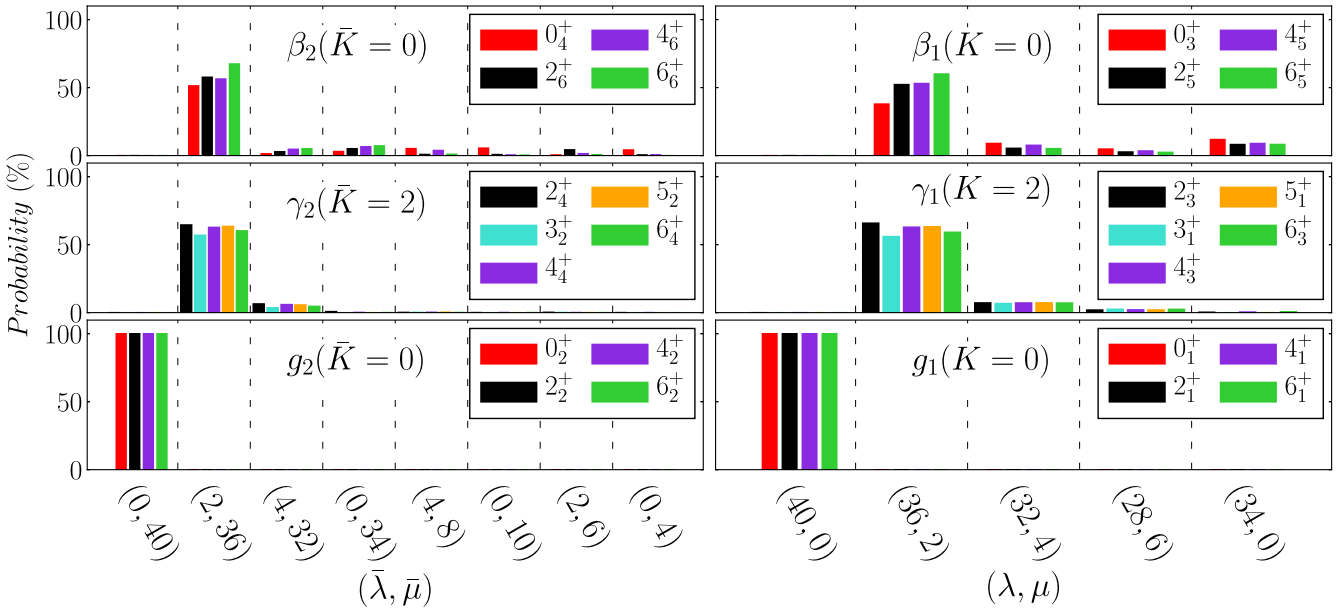

Figure 5. SU(3) (λ, μ)- and $\overline{\text{SU(3)}}$ $(\bar{\lambda}, \bar{\mu})$-decompositions for members of the prolate (g_1, β_1, γ_1) and oblate (g_2, β_2, γ_2) bands, eigenstates of $\hat{H}'$ (33) with parameters as in figure 4, resulting in P-O shape coexistence. Shown are probabilities larger than 4%. States in the prolate (g_1) and oblate (g_2) ground bands are pure with respect to SU(3) and $\overline{\text{SU(3)}}$, respectively. In contrast, excited prolate and oblate bands are mixed, thus demonstrating the presence in the spectrum of SU(3)-PDS and $\overline{\text{SU(3)}}$-PDS.

$\bar{\theta}_2 = -\hat{C}_2[\overline{\text{SU(3)}}] + 2\hat{N}(2\hat{N}+3)$, leads to similar effects but interchanges the role of prolate and oblate bands. Identifying the collective part with $\hat{C}_2[\text{SO(3)}]$, we arrive at the following complete Hamiltonian:

$$\hat{H}' = h_0\, P_0^\dagger \hat{n}_s P_0 + h_2\, P_0^\dagger \hat{n}_d P_0 + \eta_3\, G_3^\dagger \cdot \tilde{G}_3 + \alpha\, \hat{\theta}_2 + \rho\, \hat{C}_2[\text{SO(3)}]. \quad (33)$$

The prolate g_1-band remains solvable with energy $E_{g1}(L) = \rho L(L+1)$. The oblate g_2-band experiences a slight shift of order $\frac{32}{9}\alpha N^2$ and displays a rigid-rotor like spectrum. The SU(3) and $\overline{\text{SU(3)}}$ decomposition in figure 5 demonstrates that these bands are pure DS basis states, with $(2N, 0)$ and $(0, 2N)$ character, respectively, while excited β and γ bands exhibit considerable mixing. The critical-point Hamiltonian thus has a subset of states with good SU(3) symmetry, a subset of states with good $\overline{\text{SU(3)}}$ symmetry and all other states are mixed with respect to both SU(3) and $\overline{\text{SU(3)}}$. These are precisely the defining ingredients of SU(3)-PDS coexisting with $\overline{\text{SU(3)}}$-PDS.

Since the wave functions for the members of the g_1 and g_2 bands are known, one can derive analytic expressions for their quadrupole moments and $E2$ transition rates. Considering the $E2$ operator $T(E2) = e_B\, \Pi^{(2)}$ with

$$\Pi^{(2)} = d^\dagger s + s^\dagger \tilde{d}, \quad (34)$$

the quadrupole moments are found to have equal magnitudes and opposite signs,

$$Q_L = \mp e_B \sqrt{\tfrac{16\pi}{40}}\, \frac{L}{2L+3}\, \frac{4(2N-L)(2N+L+1)}{3(2N-1)}, \quad (35)$$

where the minus (plus) sign corresponds to the prolate g_1 (oblate g_2) band. The $B(E2)$ values for intraband ($g_1 \to g_1$, $g_2 \to g_2$) transitions,

$$B(E2; g_i, L+2 \to g_i, L) = e_B^2\, \frac{3(L+1)(L+2)}{2(2L+3)(2L+5)}\, \frac{(4N-1)^2(2N-L)(2N+L+3)}{18(2N-1)^2}, \quad (36)$$

are the same. These properties are ensured by the fact that $\mathcal{R}_s T(E2) \mathcal{R}_s^{-1} = -T(E2)$. Interband ($g_2 \leftrightarrow g_1$) $E2$ transitions, are extremely weak. This follows from the fact that the L-states of the g_1 and g_2 bands exhaust, respectively, the $(2N, 0)$ and $(0, 2N)$ irrep of SU(3) and $\overline{\text{SU(3)}}$. $T(E2)$ contains a (2, 2)

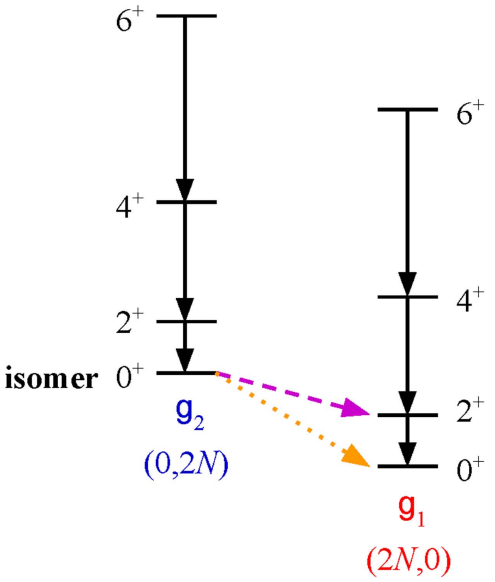

Figure 6. Signatures of SU(3) and $\overline{\text{SU(3)}}$ PDSs in P-O shape coexistence. Strong intraband $E2$ transitions (solid lines) obey the analytic expression of equation (36). Retarded $E2$ (dashed lines) and $E0$ (dotted lines) decays identify isomeric states.

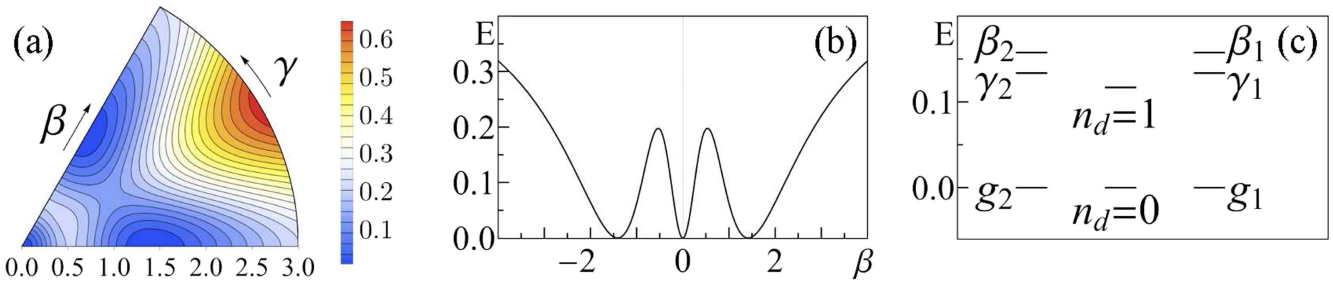

Figure 7. Spherical-prolate-oblate (S-P-O) shape coexistence. (a) Contour plots of the energy surface (40), (b) $\gamma = 0$ sections, and (c) bandhead spectrum, for the Hamiltonian $\hat{H}'$ (42) with parameters $h_2 = 0.5$, $\eta_3 = 0.567$, $\alpha = 0.018$, $\rho = 0$ and $N = 20$.

tensor under both algebras, hence can connect the $(2N, 0)$ irrep of g_1 only with the $(2N-4, 2)$ component in g_2 which, however, is vanishingly small. The selection rule $g_1 \longleftrightarrow g_2$ is valid also for a more general $E2$ operator, obtained by including in it the operators $Q^{(2)}$ (11) or $\bar{Q}^{(2)}$ (28), since the latter, as generators, cannot mix different irreps of SU(3) or $\overline{\text{SU(3)}}$. By similar arguments, $E0$ transitions in-between the g_1 and g_2 bands are extremely weak, since the relevant operator, $T(E0) \propto \hat{n}_d$, is a combination of $(0, 0)$ and $(2, 2)$ tensors under both algebras. Accordingly, the $L = 0$ bandhead state of the higher (g_2) band, cannot decay by strong $E2$ or $E0$ transitions to the lower g_1 band, hence, as depicted schematically in figure 6, displays characteristic features of an isomeric state. In contrast to g_1 and g_2, excited β and γ bands are mixed, hence are connected by $E2$ transitions to these ground bands. Their quadrupole moments are found numerically to resemble, for large N, the collective model expression $Q(K, L) = \frac{3K^2 - L(L+1)}{(L+1)2L+3)} q_K$, with $q_K > 0$ $(q_K < 0)$ for prolate (oblate) bands.

6. Triple spherical-prolate-oblate coexistence: U(5)-SU(3)-$\overline{\text{SU(3)}}$ PDS

Nuclei can accommodate more than two shapes simultaneously, as encountered in the triple coexistence of spherical, prolate and oblate shapes. The relevant DS limits for the latter configurations are [31],

$$\text{U(6)} \supset \text{U(5)} \supset \text{SO(5)} \supset \text{SO(3)} \qquad |N, n_d, \tau, n_\Delta, L\rangle. \tag{37a}$$

$$\text{U(6)} \supset \text{SU(3)} \supset \text{SO(3)} \qquad |N, (\lambda, \mu), K, L\rangle, \tag{37b}$$

$$\text{U(6)} \supset \overline{\text{SU(3)}} \supset \text{SO(3)} \qquad |N, (\bar{\lambda}, \bar{\mu}), \bar{K}, L\rangle. \tag{37c}$$

Properties of the above U(5), SU(3) and $\overline{\text{SU(3)}}$ DS chains were discussed in sections 4–5. The intrinsic part of the critical-point Hamiltonian is now required to satisfy three conditions:

$$\hat{H}|N, n_d = 0, \tau = 0, L = 0\rangle = 0, \tag{38a}$$

$$\hat{H}|N, (\lambda, \mu) = (2N, 0), K = 0, L\rangle = 0, \tag{38b}$$

$$\hat{H}|N, (\bar{\lambda}, \bar{\mu}) = (0, 2N), \bar{K} = 0, L\rangle = 0. \tag{38c}$$

Equivalently, $\hat{H}$ annihilates the spherical intrinsic state of equation (3) with $\beta = 0$, which is the single basis state in the U(5) irrep $n_d = 0$, and the deformed intrinsic states with $(\beta = \sqrt{2}, \gamma = 0)$ and $(\beta = -\sqrt{2}, \gamma = 0)$, which are the lowest and highest-weight vectors in the irreps $(2N, 0)$ and $(0, 2N)$ of SU(3) and $\overline{\text{SU(3)}}$, respectively. The resulting Hamiltonian is found to be that of equation (30) with $h_0 = 0$ [60],

$$\hat{H} = h_2 P_0^\dagger \hat{n}_d P_0 + \eta_3 G_3^\dagger \cdot \tilde{G}_3. \tag{39}$$

The corresponding energy surface, $E_N(\beta, \gamma) = N(N-1)(N-2)\tilde{E}(\beta, \gamma)$, is given by

$$\tilde{E}(\beta, \gamma) = \beta^2[\, h_2(\beta^2 - 2)^2 + \eta_3 \beta^4 \sin^2(3\gamma)](1 + \beta^2)^{-3}. \tag{40}$$

For $h_2, \eta_3 \geqslant 0$, $\hat{H}$ is positive definite and $\tilde{E}(\beta, \gamma)$ has three degenerate global minima: $\beta = 0$, $(\beta = \sqrt{2}, \gamma = 0)$ and $(\beta = \sqrt{2}, \gamma = \pi/3)$ [or equivalently $(\beta = -\sqrt{2}, \gamma = 0)$], at $\tilde{E} = 0$. Additional extremal points include (i) a saddle point: $[\beta_*^2 = \frac{2}{7}, \gamma = 0, \pi/3]$, at $\tilde{E} = \frac{32}{81} h_2$. (ii) A local maximum and a saddle point: $[\beta_{**}^2, \gamma = \pi/6]$, at $\tilde{E} = \frac{4}{3} h_2 (1 + \beta_{**}^2)^{-2} \beta_{**}^2 (2 - \beta_{**}^2)$, where β_{**}^2 is a solution of $(7h_2 + 3\eta_3)\beta_{**}^4 - 16h_2\beta_{**}^2 + 4h_2 = 0$. The saddle points, when they exist, support a barrier separating the various minima, as seen in figure 7. The normal modes involve quadrupole vibrations about the spherical minimum with frequency ϵ alongside β and γ vibrations about the deformed prolate and oblate minima with frequencies $\epsilon_{\beta i}$ and $\epsilon_{\gamma i}$,

$$\epsilon = 4h_2 N^2, \tag{41a}$$

$$\epsilon_{\beta 1} = \epsilon_{\beta 2} = \frac{16}{3} h_2 N^2, \tag{41b}$$

$$\epsilon_{\gamma 1} = \epsilon_{\gamma 2} = 4\eta_3 N^2. \tag{41c}$$

The spherical modes are seen to have a lower frequency than the β modes, $\epsilon = \frac{3}{4}\epsilon_{\beta i}$. Figures 7(a), (b) and (c) show $\tilde{E}(\beta, \gamma)$, $\tilde{E}(\beta, \gamma = 0)$ and the normal-mode spectrum with parameters ensuring spherical-prolate-oblate (S-P-O) minima.

For the same arguments as in the analysis of prolate-oblate shape coexistence in section 5, the complete Hamiltonian is taken to be

$$\hat{H}' = h_2 P_0^\dagger \hat{n}_d P_0 + \eta_3 G_3^\dagger \cdot \tilde{G}_3 + \alpha \hat{\theta}_2 + \rho \hat{C}_2[\text{SO(3)}]. \tag{42}$$

The deformed bands show similar rigid-rotor structure as in the P-O case. In particular, the prolate g_1-band and oblate g_2-band have good SU(3) and $\overline{\text{SU(3)}}$ symmetry, respectively,

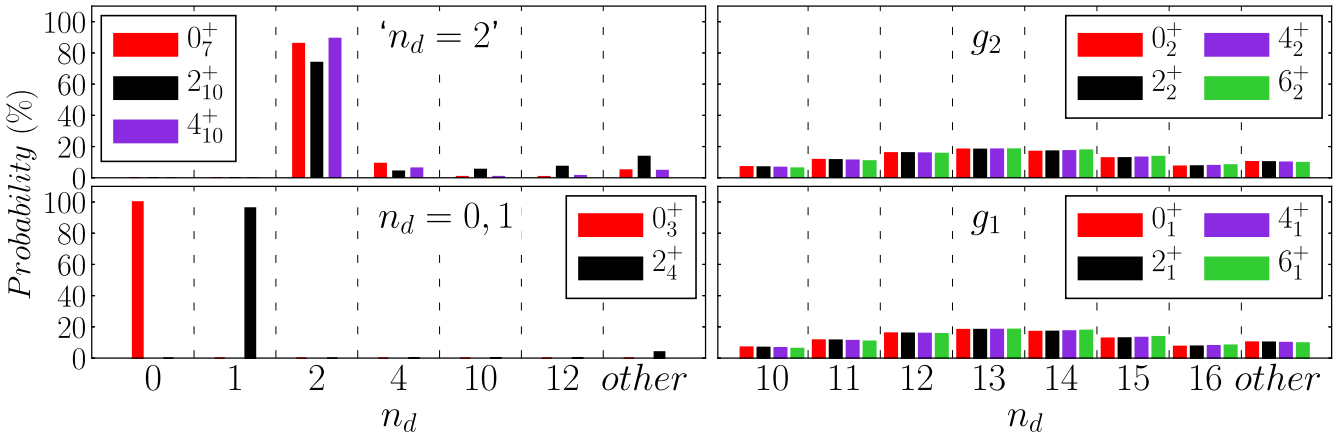

Figure 8. U(5) n_d-decomposition for spherical states (left panels) and for members of the deformed prolate (g_1) and oblate (g_2) ground bands (right panels), eigenstates of $\hat{H}'$ (42) with parameters as in figure 7, resulting in S-P-O shape coexistence. The column 'other' depicts a sum of probabilities, each less than 5%. The spherical states are dominated by a single n_d component, in marked contrast to the deformed states, thus signaling the presence in the spectrum of U(5)-PDS.

while excited β and γ bands exhibit considerable mixing, with similar decompositions as in figure 5. A new aspect in the present S-P-O case, is the simultaneous occurrence in the spectrum (see figure 7(c)) of spherical type of states, whose wave functions are dominated by a single n_d component. As shown in the left panels of figure 8, the lowest spherical $L = 0_3^+$ state is a pure $n_d = 0$ state, which is the solvable U(5) basis state of equation (38*a*). The $L = 2_4^+$ state is almost pure, with a probability of 96.1% for the $n_d = 1$ component. The origin of its high degree of purity can be traced to the relation

$$\hat{H}|N, n_d = \tau = 1, L = 2\rangle = h_2\, 4(N-1)(N-2)\Big[|N, n_d = \tau = 1, L = 2\rangle - \sqrt{\tfrac{7}{2(N-1)(N-2)}}\,|N, n_d = \tau = L = 2\rangle\Big], \quad (43)$$

which shows that the U(5) basis state $|N, n_d = \tau = 1, L = 2\rangle$ approaches the status of an eigenstate for large N, with corrections of order $1/N$. Higher spherical type of states ($L = 0_7^+, 2_{10}^+, 4_{10}^+$) have a pronounced ($\sim 80\%$) $n_d = 2$ component. This structure should be contrasted with the U(5) decomposition of deformed states (e.g., those belonging to the g_1 and g_2 bands) which, as shown in the right panels of figure 8, have a broad n_d-distribution. The purity of selected sets of states with respect to SU(3), $\overline{\text{SU(3)}}$ and U(5) as demonstrated in figures 5 and 8, in the presence of other mixed states, are the hallmarks of coexisting SU(3)-PDS, $\overline{\text{SU(3)}}$-PDS and U(5)-PDS. It is remarkable that a simple Hamiltonian, as in equation (42), can accommodate simultaneously several incompatible symmetries in a segment of its spectrum.

Considering the same $E2$ operator $T(E2) = e_B\Pi^{(2)}$, equation (34), as in the P-O case of section 5, the quadrupole moments of states in the solvable g_1 and g_2 bands and intraband ($g_1 \to g_1$, $g_2 \to g_2$) $E2$ rates, obey the analytic expressions of equations (35) and (36), respectively. The same selection rules depicted in figure 6, resulting in retarded $E2$ and $E0$ interband ($g_2 \to g_1$) decays, are still valid. Furthermore, in the current S-P-O case, since $T(E2)$ obeys the selection rule

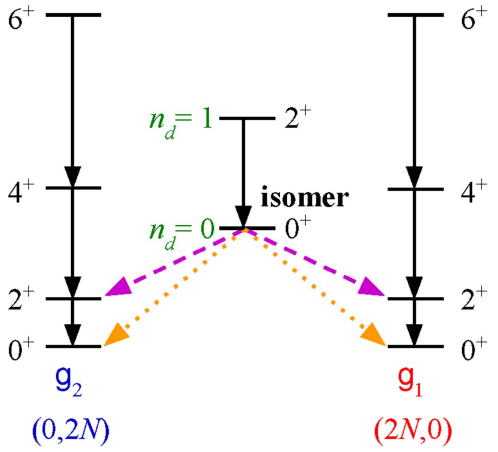

Figure 9. Signatures of U(5), SU(3) and $\overline{\text{SU(3)}}$ PDSs in S-P-O shape coexistence. Strong intraband $E2$ transitions (solid lines) obey the analytic expressions of equations (36) and (44). Retarded $E2$ (dashed lines) and $E0$ (dotted lines) decays identify isomeric states.

$\Delta n_d = \pm 1$, the spherical states, ($n_d = L = 0$) and ($n_d = 1, L = 2$), have no quadrupole moment and the $B(E2)$ value for their connecting transition, obeys the U(5)-DS expression [31]

$$B(E2; n_d = 1, L = 2 \to n_d = 0, L = 0) = e_B^2 N. \quad (44)$$

These spherical states have very weak $E2$ transitions to the deformed ground bands, because they exhaust the ($n_d = 0, 1$) irreps of U(5), and the $n_d = 2$ component in the ($L = 0, 2, 4$) states of the g_1 and g_2 bands is extremely small, of order $N^3 3^{-N}$, as can be inferred from equation (24). There are also no $E0$ transitions involving these spherical states, since $T(E0)$ is diagonal in n_d.

In the above analysis the spherical and deformed minima were assumed to be near degenerate. If the spherical minimum is only local, one can use the Hamiltonian of equation (33) with the condition $h_2 > 4h_0$, for which the spherical ground state ($n_d = L = 0$) experiences a shift of order $4h_0N^3$. Similarly, if the deformed minima are only

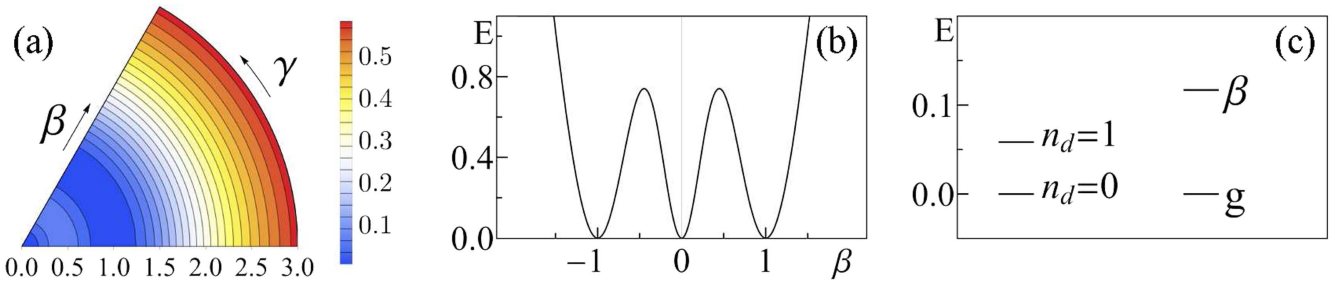

Figure 10. Spherical and γ-unstable deformed (S-G) shape coexistence. (a) Contour plots of the γ-independent energy surface (51), (b) $\gamma = 0$ sections, and (c) bandhead spectrum, for the Hamiltonian $\hat{H}'$ (53) with parameters $r_2 = 1$, $\rho_5 = \rho_3 = 0$, and $N = 20$.

local, adding an $\epsilon \hat{n}_d$ term to $\hat{H}'$ (42), will leave the $n_d = 0$ spherical ground state unchanged, but will shift the prolate and oblate bands to higher energy of order $2\epsilon N/3$. In both scenarios, the lowest $L = 0$ state of the non-yrast configuration will exhibit retarded $E2$ and $E0$ decays, hence will have the attributes of an isomer state, as depicted schematically in figure 9.

7. Spherical and γ-unstable deformed shape coexistence: U(5)-SO(6) PDS

The γ degree of freedom and triaxiality can play an important role in the occurrence of multiple shapes in nuclei [79]. In the present section, we examine the coexistence of a spherical shape and a particular type of non-axial deformed shape, which is γ-soft. The relevant DS chains for such configurations are [31],

$$\mathrm{U}(6) \supset \mathrm{U}(5) \supset \mathrm{SO}(5) \supset \mathrm{SO}(3) \qquad |N, n_d, \tau, n_\Delta, L\rangle, \tag{45a}$$

$$\mathrm{U}(6) \supset \mathrm{SO}(6) \supset \mathrm{SO}(5) \supset \mathrm{SO}(3) \qquad |N, \sigma, \tau, n_\Delta, L\rangle. \tag{45b}$$

The U(5)-DS limit (45*a*), appropriate to a spherical shape, was discussed in section 4. The SO(6)-DS limit (45*b*) is appropriate to the dynamics of a γ-unstable deformed shape. For a given U(6) irrep N, the allowed SO(6) and SO(5) irreps are $\sigma = N, N-2, \ldots 0$ or 1, and $\tau = 0, 1, \ldots \sigma$, respectively. The SO(5) $\supset$ SO(3) reduction is the same as in the U(5)-DS chain. The basis states are eigenstates of the Casimir operator $\hat{C}_2[\mathrm{SO}(6)] = 2\Pi^{(2)} \cdot \Pi^{(2)} + \hat{C}_2[\mathrm{SO}(5)]$ with eigenvalues $\sigma(\sigma+4)$. The generators of SO(6) are the angular momentum, octupole and quadrupole operators, $L^{(1)}$, $(d^\dagger \tilde{d})^{(3)}$ and $\Pi^{(2)}$, equation (34). The SO(6)-DS spectrum resembles that of a γ-unstable deformed rotovibrator, composed of SO(6) σ-multiplets forming rotational bands, with $\tau(\tau+3)$ and $L(L+1)$ splitting generated by $\hat{C}_2[\mathrm{SO}(5)]$ and $\hat{C}_2[\mathrm{SO}(3)]$, respectively. The lowest irrep $\sigma = N$ contains the ground (g) band of a γ-unstable deformed nucleus. The first excited irrep $\sigma = N-2$ contains the β-band. The lowest members in each band have quantum numbers $(\tau = 0, L = 0)$, $(\tau = 1, L = 2)$, $(\tau = 2, L = 2, 4)$ and $(\tau = 3, L = 0, 3, 4, 6)$.

In discussing the properties of the SO(6)-DS spectrum, it is convenient to subtract from $\hat{C}_2[\mathrm{O}(6))]$ the ground-state energy, and consider the following positive-definite term:

$$R_0^\dagger R_0 = -\hat{C}_2[\mathrm{SO}(6)] + \hat{N}(\hat{N}+4). \tag{46}$$

The SO(6) basis states $|N, \sigma, \tau, n_\Delta, L\rangle$, equation (45*b*), are then eigenstates of $R_0^\dagger R_0$ with eigenvalues $(N-\sigma)(N+\sigma+4)$, and the ground band with $\sigma = N$ occurs at zero energy. The two-boson pair operator

$$R_0^\dagger = d^\dagger \cdot d^\dagger - (s^\dagger)^2, \tag{47}$$

is a scalar with respect to SO(6) and satisfies

$$R_0\,|N, \sigma = N, \tau, n_\Delta, L\rangle = 0. \tag{48}$$

This operator corresponds to $\hat{T}_\alpha$ of equation (7) and, as shown below, it plays a central role in the construction of Hamiltonians with SO(6)-PDS.

The phase transition between spherical and γ-unstable deformed shapes, has been previously studied by varying a control parameter in an IBM Hamiltonian mixing the U(5) and SO(6) Casimir operators [37, 67, 68, 80]. However, the latter employed one- and two-body terms, hence the resulting quantum phase transition is of second order, where one minimum evolves continuously to the second minimum. To allow for a first-order quantum phase transition, involving coexisting shapes, we consider an Hamiltonian with cubic terms which retains the virtues of U(5) and SO(6) DSs for the spherical ground state and the γ-unstable deformed ground band, respectively. Following the procedure outlined in equation (9), the intrinsic part of the critical-point Hamiltonian is required to satisfy

$$\hat{H}|N, \sigma = N, \tau, L\rangle = 0 \qquad \tau = 0, 1, 2, \ldots, N \tag{49a}$$

$$\hat{H}|N, n_d = 0, \tau = 0, L = 0\rangle = 0. \tag{49b}$$

Equivalently, $\hat{H}$ annihilates both the deformed intrinsic state of equation (3) with ($\beta = 1$, γ arbitrary), which is the lowest weight vector in the SO(6) irrep $\sigma = N$, and the spherical intrinsic state with $\beta = 0$, which is the single basis state in the U(5) irrep $n_d = 0$. The resulting Hamiltonian is found to be

$$\hat{H} = r_2\, R_0^\dagger \hat{n}_d R_0, \tag{50}$$

where $R_0^\dagger$ is given in equation (47). The energy surface, $E_N(\beta, \gamma) = N(N-1)(N-2)\tilde{E}(\beta, \gamma)$, is given by

$$\tilde{E}(\beta) = r_2 \beta^2 (\beta^2 - 1)^2 (1+\beta^2)^{-3}. \tag{51}$$

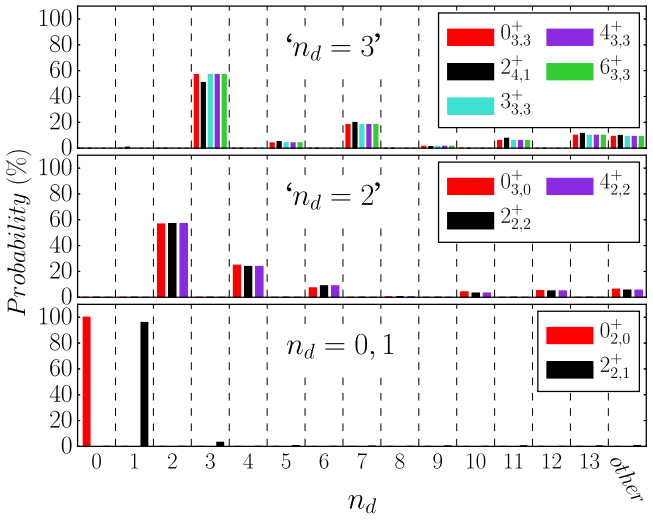

Figure 11. U(5) n_d-decomposition for spherical states, eigenstates of the Hamiltonian $\hat{H}'$ (53) with parameters as in figure 10. The column 'other' depicts a sum of probabilities, each less than 5%.

The surface is an even sextic function of β and is independent of γ, in accord with the SO(5) symmetry of the Hamiltonian. It has the form $\tilde{E}(\beta) = (1 + \beta^2)^{-3}[A\beta^6 + D\beta^4 + F\beta^2]$, with coefficients $A = F = r_2$, $D = -2r_2$, satisfying $D^2 = 4AF$. Such a topology necessitates the presence of cubic terms in the Hamiltonian, and the latter condition ensures that the surface supports two degenerate extrema, spherical and deformed. For $r_2 > 0$, $\hat{H}$ is positive definite and $\tilde{E}(\beta)$ has two degenerate global minima, $\beta = 0$ and $\beta^2 = 1$, at $\tilde{E} = 0$. A local maximum at $\beta^2_* = \frac{1}{5}$ creates a barrier of height $\tilde{E} = \frac{2}{27}r_2$, separating the two minima, as seen in figure 10. For large N, the normal modes shown schematically in figure 10(c), involve β vibrations about the deformed minima, with frequency ϵ_β, and quadrupole vibrations about the spherical minimum, with frequency ϵ, respectively,

$$\epsilon_\beta = 2r_2\, N^2, \tag{52a}$$

$$\epsilon = r_2\, N^2. \tag{52b}$$

Interestingly, the β mode has twice the energy of the spherical modes, $\epsilon_\beta = 2\epsilon$, compared to equal energies encountered in the case of spherical-prolate coexistence (see equations (18*a*) and (19)).

Identifying the collective part of the Hamiltonian with the Casimir operators of the common SO(5) $\supset$ SO(3) segment of the chains (45), we arrive at the following complete Hamiltonian

$$\hat{H}' = r_2\, R_0^\dagger \hat{n}_d R_0 + \rho_5\, \hat{C}_2[\mathrm{SO}(5)] + \rho_3\, \hat{C}_2[\mathrm{SO}(3)]. \tag{53}$$

The added rotational terms generate an exact $\rho_5\tau(\tau + 3) + \rho_3 L(L + 1)$ splitting without affecting the wave functions. In particular, the solvable subset of eigenstates, equation (49), remain intact. Since both SO(5) and SO(3) are preserved by the Hamiltonian, its eigenstates have good (τ, L) quantum numbers and can be labeled as $L^+_{i,\tau}$, where the ordinal number i enumerates the occurrences of states with the same (τ, L) with increasing energy. The nature of the Hamiltonian

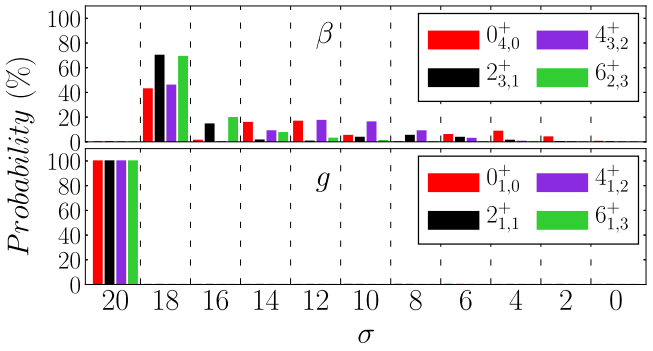

Figure 12. SO(6) σ-decomposition for members of the deformed ground (g) and β bands, eigenstates of the Hamiltonian $\hat{H}'$ (53) with parameters as in figure 10, resulting in S-G shape coexistence.

eigenstates can be inferred from the probability distributions, $P^{(N,\tau,L)}_{n_d} = |C^{(N,\tau,L)}_{n_d}|^2$ and $P^{(N,\tau,L)}_{\sigma} = |C^{(N,\tau,L)}_{\sigma}|^2$, obtained from their expansion coefficients in the U(5) and SO(6) bases (45). In general, the low-lying spectrum of $\hat{H}'$ (53) exhibits two distinct classes of states. The first class consists of (τ, L) states arranged in n_d-multiplets of a spherical vibrator. Figure 11 shows the U(5) n_d-decomposition of such spherical states, characterized by a narrow n_d-distribution. The lowest spherical state, $L = 0^+_{2,0}$, is the solvable U(5) state of equation (49*b*) with U(5) quantum number $n_d = 0$. The $L = 2^+_{2,1}$ state has $n_d = 1$ to a good approximation. Its high purity can be traced to the relation

$$\begin{aligned}\hat{H}|N, n_d = \tau = 1, L = 2\rangle \\ = r_2(N-1)(N-2)\Big[|N, n_d = \tau = 1, L = 2\rangle \\ - \sqrt{\tfrac{14}{(N-1)(N-2)}}\,|N, n_d = \tau = L = 2\rangle\Big],\end{aligned} \tag{54}$$

which shows that the U(5)-basis state $|N, n_d = \tau = 1, L = 2\rangle$ is almost an eigenstate for large N, with corrections of order $1/N$. The upper panels of figure 11 display the next spherical type of multiplets ($L = 0^+_{3,0}, 2^+_{2,2}, 4^+_{2,2}$) and ($L = 6^+_{3,3}, 4^+_{3,3}, 3^+_{3,3}, 0^+_{3,3}, 2^+_{4,1}$), which have a somewhat less pronounced (60%) single n_d-component, with $n_d = 2$ and $n_d = 3$, respectively.

A second class consists of (τ, L) states arranged in bands of a γ-unstable deformed rotor. The SO(6) σ-decomposition of such states, in selected bands, are shown in figure 12. The ground band is seen to be pure with $\sigma = N$ SO(6) character, and coincides with the solvable band of equation (49*a*). In contrast, the non-solvable β-band (and higher β^n-bands) show considerable SO(6)-mixing. The deformed nature of these SO(5)-rotational states is manifested in their broad n_d-distribution, shown in figure 13. This is explicitly evident in the following expansion of the SO(6) ground band wave functions in the U(5) basis,

$$\begin{aligned}|N, \sigma = N, \tau, n_\Delta, L\rangle = \sum_{n_d} \frac{1}{2}[1 + (-1)^{n_d - \tau}] \\ \times\, \theta^{(N,\tau)}_{n_d} |N, n_d, \tau, n_\Delta, L\rangle,\end{aligned} \tag{55a}$$

$$\theta^{(N,\tau)}_{n_d} = \left[\frac{(N-\tau)!(N+\tau+3)!}{2^{N+1}(N+1)!(N-n_d)!(n_d-\tau)!!(n_d+\tau+3)!!}\right]^{1/2}, \tag{55b}$$

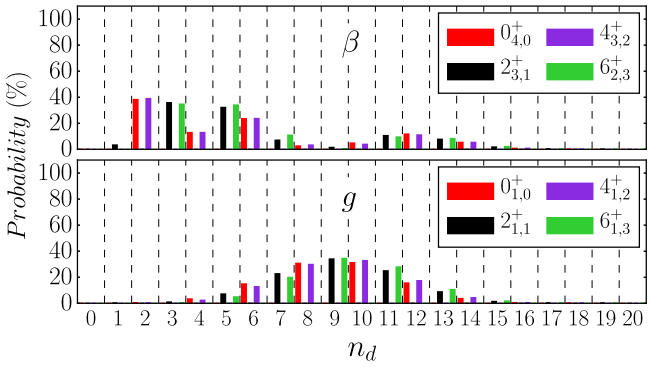

Figure 13. U(5) n_d-decomposition for members of the deformed ground (g) and β bands, eigenstates of the Hamiltonian $\hat{H}'$ (53) with parameters as in figure 10, resulting in spherical and γ-unstable deformed (S-G) shape coexistence. The results of figures 11–13, demonstrate the presence in the spectrum of U(5)-PDS and SO(6)-PDS.

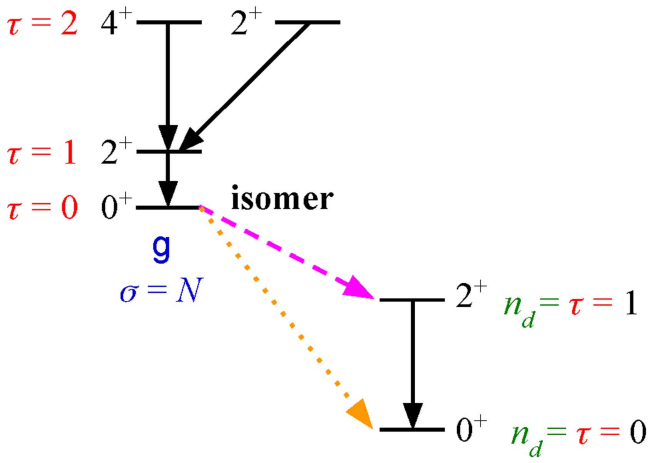

Figure 14. Signatures of U(5) and SU(6) PDSs in S-G shape coexistence. Strong intraband E2 transitions (solid lines) obey the analytic expressions of equations (44) and (56). Retarded E2 (dashed lines) and E0 (dotted lines) decays identify isomeric states.

which shows that for large N, the probability of each individual n_d component is exponentially small. The above analysis demonstrates that although the critical-point Hamiltonian (53) is not invariant under U(5) nor SO(6), some of its eigenstates have good U(5) symmetry, some have good SO(6) symmetry and all other states are mixed with respect to both U(5) and SO(6). These are precisely the defining attributes of U(5)-PDS coexisting with SO(6)-PDS.

Since the wave functions for the solvable states, equations (49), are known, one has at hand closed form expressions for related spectroscopic observables. Considering the $E2$ operator $T(E2) = e_B\,\Pi^{(2)}$ with $\Pi^{(2)}$ given in equation (34), it obeys the SO(5) selection rules $\Delta\tau = \pm 1$ and, consequently, all (τ, L) states have vanishing quadrupole moments. The $B(E2)$ values for intraband $(g \to g)$ transitions between states of the ground band, equation (49a), are given by the known SO(6)-DS expressions [31]. For example,

$$B(E2; g, \tau+1, L' = 2\tau+2 \to g, \tau, L = 2\tau) = e_B^2\,\frac{\tau+1}{2\tau+5}(N-\tau)(N+\tau+4), \quad (56a)$$

$$B(E2; g, \tau+1, L' = 2\tau \to g, \tau, L = 2\tau) = e_B^2\,\frac{4\tau+2}{(2\tau+5)(4\tau-1)}(N-\tau)(N+\tau+4). \quad (56b)$$

Similarly, the $E2$ rates for the transition connecting the pure spherical states, $(n_d = \tau = 1, L = 2)$ and $(n_d = \tau = 0, L = 0)$, satisfy the U(5)-DS expression of equation (44). Member states of the deformed ground band (49a) span the entire $\sigma = N$ irrep of SO(6) and are not connected by $E2$ transitions to the spherical states since $\Pi^{(2)}$, as a generator of SO(6), cannot connect different σ-irreps of SO(6). The weak spherical $\to$ deformed $E2$ transitions persist also for a more general $E2$ operator obtained by adding $(d^\dagger\tilde{d})^{(2)}$ to $T(E2)$, since the latter term, as a generator of U(5), cannot connect different n_d-irreps of U(5). By similar arguments, there are no $E0$ transitions involving these spherical states, since $T(E0)$ is diagonal in n_d. These symmetry-based selection rules result in strong electromagnetic transitions between states in the same class, associated with a given shape, and weak transitions between states in different classes, hence can be used to identify isomeric states.

The evolution of structure away from the critical point, where the spherical and deformed configurations are degenerate, can be studied by incorporating the U(5) or SO(6) Casimir operators in $\hat{H}'$ (53), still retaining the desired SO(5) symmetry. Adding an $\epsilon\hat{n}_d$ term, will leave the pure spherical $n_d = 0, 1$ states unchanged but will shift the deformed γ-unstable ground band to higher energy of order $\epsilon N/3$. Similarly, adding a small $\alpha R_0^\dagger R_0$ term (46), will leave the solvable SO(6) $\sigma = N$ ground band unchanged, but will shift the spherical ground state ($n_d = L = 0$) to higher energy of order αN^2. As discussed, the $L = 0$ state of the excited configuration will exhibit retarded $E2$ and $E0$ decays to states of the lower configuration, hence will have the attributes of an isomer state, as depicted schematically in figure 14.

8. Concluding remarks

We have presented a comprehensive symmetry-based approach for describing properties of multiple shapes in the framework of the interacting boson model (IBM) of nuclei. It involves the construction of a number-conserving rotational-invariant Hamiltonian which captures the essential features of the dynamics near the critical point, where two (or more) shapes coexist. The Hamiltonian conserves the DS of selected bands, associated with each shape. Since different structural phases correspond to incompatible (non-commuting) dynamical symmetries, the symmetries in question are shared by only a subset of states, and are broken in the remaining eigenstates of the Hamiltonian. The resulting structure is, therefore, that of coexisting multiple PDSs.

We have applied the proposed approach and examined the relevance of the PDS notion to a rich variety of multiple quadrupole shapes, spherical and deformed (axial and non-axial). The shape coexistence scenarios and related PDSs considered include (i) U(5)-PDS and SU(3)-PDS in relation

to spherical-prolate coexistence. (ii) SU(3)-PDS and $\overline{\text{SU(3)}}$-PDS in relation to prolate-oblate coexistence. (iii) U(5)-PDS, SU(3)-PDS and $\overline{\text{SU(3)}}$-PDS in relation to triple spherical-prolate-oblate coexistence. (iv) U(5)-PDS and SO(6)-PDS in relation to coexisting spherical and γ-unstable deformed shapes. In each case, the underlying potential-energy surface exhibits multiple minima which are near degenerate. As shown, the constructed Hamiltonian has the capacity to have distinct families of states whose properties reflect the different nature of the coexisting shapes. Selected sets of states within each family, retain the dynamical symmetry associated with the given shape. This allows one to obtain closed expressions for quadrupole moments and transition rates, which are the observables most closely related to the nuclear shape. The resulting analytic expressions, (equations (25), (26), (35), (36), (44), (56)), are parameter-free predictions, except for a scale, and can be used to compare with measured values of these observables and to test the underlying partial symmetries. The purity and good quantum numbers of selected states enable the derivation of symmetry-based selection rules for electromagnetic transitions (notably, for $E2$ and $E0$ decays) and the subsequent identification of isomeric states. The evolution of structure away from the critical-point can be studied by adding to the Hamiltonian the Casimir operator of a particular DS chain, which will leave unchanged the ground band of one configuration but will shift the other configuration(s) to higher energy and may alter their symmetry properties.

The critical-point Hamiltonians obtained in the procedure of equation (9), often involve three-body interactions. Similar cubic terms were encountered in previous studies within the IBM, in conjunction with triaxiality [81, 82], band anharmonicity [49, 83] and signature splitting [50, 84] in deformed nuclei. Higher-order terms show up naturally in microscopic-inspired IBM Hamiltonians derived by a mapping from self-consistent mean-field calculations [24, 85]. Near shell-closure such critical-point Hamiltonian can be regarded as an effective number-conserving Hamiltonian, which simulates the excluded intruder configurations by means of higher-order terms. Indeed, the energy surfaces of the IBM with configuration mixing [20, 21, 86] contain higher-powers of β^2 and $\beta^3\cos 3\gamma$, as in equation (31). Recalling the microscopic interpretation of the IBM bosons as images of identical valence–nucleon pairs, the results of the present study suggest that for nuclei far from shell-closure, shape coexistence can occur within the same valence space.

As discussed, the yrast states of each coexisting configuration, (e.g., the prolate and oblate ground bands) are unmixed and retain their individual symmetry character (e.g., the SU(3) and $\overline{\text{SU(3)}}$ character). This situation is different from that encountered in the neutron-deficient Kr [4] and Hg [6] isotopes, where the observed structures are strongly mixed. It is in line with the recent evidence for shape coexistence in neutron-rich Sr isotopes, where spherical and prolate-deformed configurations exhibit very weak mixing [8]. Band mixing can be incorporated in the present formalism by adding kinetic rotational terms which do not affect the shape of the energy surface [69–71, 78]. For an Hamiltonian with one-, two- and three-body terms, the rotational terms are of three types. (A) Operators related to the Casimir operators $\hat{C}_2[G]$ of the groups (G) in the chain $\overline{SO(6)} \supset SO(5) \supset SO(3)$, where the generators of $\overline{SO(6)}$ are $U^{(\ell)} = (d^\dagger\tilde{d})^{(\ell)}$, $\ell = 1, 3$ and $\overline{\Pi}^{(2)} = i(d^\dagger s - s^\dagger\tilde{d})$. These orthogonal groups correspond to 'generalized' rotations associated with the β-, γ-, and Euler angles degrees of freedom [70]. (B) Operators of the form $\hat{n}_d\hat{C}_2[G]$. (C) Operators of the form $\Pi^{(2)}\cdot(\overline{\Pi}^{(2)}\,\overline{\Pi}^{(2)})^{(2)}$, $\Pi^{(2)}\cdot(U^{(1)}\,U^{(1)})^{(2)}$, $U^{(2)}\cdot(U^{(1)}\,U^{(1)})^{(2)}$, $i\overline{\Pi}^{(2)}\cdot(U^{(2)}\,U^{(3)})^{(2)}$ and their Hermitian conjugates. Operators in classes (A) and (B) are diagonal in the SO(5) quantum number τ, while those in class (C) allow for τ mixing. Most of these rotational terms do not commute with the intrinsic part of the Hamiltonian hence can shift, split and mix the bands generated by the latter. So far, these effects were considered only for the operators of class (A) in conjunction with the coexistence of spherical and prolate-deformed shapes [66], hence a detailed systematic study of other terms is called for. It should be noted that if the induced band mixing is strong, it may destroy the PDS property of the eigenstates of the complete Hamiltonian.

Shape coexistence in an interacting system, such as nuclei, occurs as a result of a competition between terms in the Hamiltonian with different symmetry character, which leads to considerable symmetry-breaking effects in most states. To address the persisting regularities in such circumstances, amidst a complicated environment of other states, one needs to enlarge the traditional concepts of exact dynamical symmetries. The present symmetry-based approach accomplishes that by employing such an extended notion of PDS. In the same spirit that exact dynamical symmetries are known to serve as benchmarks for the dynamics of a single shape, it appears that partial dynamical symmetries have the capacity and potential to act as benchmarks for the study of multiple shapes in nuclei. PDSs can provide a convenient starting point, guidance and test-ground for more detailed treatments of this intriguing phenomena. Further work is required to quantitatively asses to what extent partial symmetries persist in real nuclei, where shape coexistence necessitates additional symmetry-breaking effects due to departures from the critical-point and band mixing. It is gratifying to note that shape coexistence in nuclei, exemplifying a quantal mesoscopic system, constitutes a fertile ground for the development and testing of generalized notions of symmetry.

Acknowledgments

This work is supported by the Israel Science Foundation (Grant 586/16).

References

[1] Heyde K and Wood J L 2011 *Rev. Mod. Phys.* **83** 1467
[2] Wood J L and Heyde K 2016 *J. Phys. G* **43** 020402
[3] Jenkins D G 2014 *Nature Phys.* **10** 909
[4] Clément E *et al* 2007 *Phys. Rev.* C **75** 054313
[5] Ljungvall J *et al* 2008 *Phys. Rev. Lett.* **100** 102502

[6] Bree N *et al* 2014 *Phys. Rev. Lett.* **112** 162701
[7] Chen S *et al* 2017 *Phys. Rev.* C **95** 041302(R)
[8] Clément E *et al* 2016 *Phys. Rev. Lett.* **116** 022701
[9] Park J *et al* 2016 *Phys. Rev.* C **93** 014315
[10] Kremer C *et al* 2016 *Phys. Rev. Lett.* **117** 172503
[11] Gottardo A *et al* 2016 *Phys. Rev. Lett.* **116** 182501
[12] Yang X F *et al* 2016 *Phys. Rev. Lett.* **116** 182502
[13] Andreyev A N *et al* 2000 *Nature* **405** 430
[14] Mizusaki T, Otsuka T, Utsuno Y, Honma M and Sebe T 1999 *Phys. Rev.* C **59** 1846(R)
[15] Tsunoda Y, Otsuka T, Shimizu N, Honma M and Utsuno Y 2014 *Phys. Rev.* C **89** 031301(R)
[16] Duval P D and Barrett B R 1981 *Phys. Lett.* B **100** 223
[17] Duval P D and Barrett B R 1982 *Nucl. Phys.* A **376** 213
[18] Sambataro M and Molnar G 1982 *Nucl. Phys.* A **376** 201
[19] Fossion R, Heyde K, Thiamova G and Van Isacker P 2003 *Phys. Rev.* C **67** 024306
[20] Frank A, Van Isacker P and Vargas C E 2004 *Phys. Rev.* C **69** 034323
[21] Morales I O, Frank A, Vargas C E and Van Isacker P 2008 *Phys. Rev.* C **78** 024303
[22] García-Ramos J E and Heyde K 2014 *Phys. Rev.* C **89** 014306
[23] Nomura K, Rodríguez-Guzmán R, Robledo L M and Shimizu N 2012 *Phys. Rev.* C **86** 034322
[24] Nomura K, Rodríguez-Guzmán R and Robledo L M 2013 *Phys. Rev.* C **87** 064313
[25] Nomura K, Otsuka T and Van Isacker P 2016 *J. Phys.* G **43** 024008
[26] Yao J M, Bender M and Heenen P H 2013 *Phys. Rev.* C **87** 034322
[27] Li Z P, Nikšić T and Vretenar D 2016 *J. Phys.* G **43** 024005
[28] Nomura K, Nikšić T, Otsuka T, Shimizu N and Vretenar D 2011 *Phys. Rev.* C **84** 014302
[29] Möller P, Sierk A J, Bengtsson R, Sagawa H and Ichikawa T 2009 *Phys. Rev. Lett.* **103** 212501
[30] Möller P, Sierk A J, Bengtsson R, Sagawa H and Ichikawa T 2009 *Atomic Data Nucl. Data Tables* **98** 149
[31] Iachello F and Arima A 1987 *The Interacting Boson Model* (Cambridge: Cambridge University Press)
[32] Iachello F 2000 *Phys. Rev. Lett.* **85** 3580
[33] Iachello F 2001 *Phys. Rev. Lett.* **87** 052502
[34] Casten R F and Zamfir N V 2000 *Phys. Rev. Lett.* **85** 3584
[35] Casten R F and Zamfir N V 2001 *Phys. Rev. Lett.* **87** 052503
[36] Ginocchio J N and Kirson M W 1980 *Phys. Rev. Lett.* **44** 1744
[37] Dieperink A E L, Scholten O and Iachello F 1980 *Phys. Rev. Lett.* **44** 1747
[38] Leviatan A 2011 *Prog. Part. Nucl. Phys.* **66** 93
[39] Alhassid Y and Leviatan A 1992 *J. Phys.* A **25** L1265
[40] Leviatan A 1996 *Phys. Rev. Lett.* **77** 818
[41] Leviatan A and Sinai I 1999 *Phys. Rev.* C **60** 061301(R)
[42] Casten R F, Cakirli R B, Blaum K and Couture A 2014 *Phys. Rev. Lett.* **113** 112501
[43] Couture A, Casten R F and Cakirli R B 2015 *Phys. Rev.* C **91** 014312
[44] Casten R F, Jolie J, Cakirli R B and Couture A 2016 *Phys. Rev.* C **94** 061303(R)
[45] Van Isacker P 1999 *Phys. Rev. Lett.* **83** 4269
[46] Leviatan A and Van Isacker P 2002 *Phys. Rev. Lett.* **89** 222501
[47] Kremer C *et al* 2014 *Phys. Rev.* C **89** 041302(R)
Kremer C *et al* 2015 *Phys. Rev.* C **92** 039902
[48] Leviatan A and Ginocchio J N 2000 *Phys. Rev.* C **61** 024305
[49] García-Ramos J E, Leviatan A and Van Isacker P 2009 *Phys. Rev. Lett.* **102** 112502
[50] Leviatan A, García-Ramos J E and Van Isacker P 2013 *Phys. Rev.* C **87** 021302(R)
[51] Escher J and Leviatan A 2000 *Phys. Rev. Lett.* **84** 1866
[52] Escher J and Leviatan A 2002 *Phys. Rev.* C **65** 054309
[53] Rowe D J and Rosensteel G 2001 *Phys. Rev. Lett.* **87** 172501
[54] Rosensteel G and Rowe D J 2003 *Phys. Rev.* C **67** 014303
[55] Van Isacker P and Heinze S 2008 *Phys. Rev. Lett.* **100** 052501
[56] Van Isacker P and Heinze S 2014 *Ann. Phys. (N.Y.)* **349** 73
[57] Van Isacker P, Jolie J, Thomas T and Leviatan A 2015 *Phys. Rev.* C **92** 011301(R)
[58] Leviatan A 2007 *Phys. Rev. Lett.* **98** 242502
[59] Macek M and Leviatan A 2014 *Ann. Phys. (N.Y.)* **351** 302
[60] Leviatan A and Shapira D 2016 *Phys. Rev.* C **93** 051302(R)
[61] Whelan N, Alhassid Y and Leviatan A 1993 *Phys. Rev. Lett.* **71** 2208
[62] Leviatan A and Whelan N D 1996 *Phys. Rev. Lett.* **77** 5202
[63] Iachello F, Zamfir N V and Casten R F 1998 *Phys. Rev. Lett.* **81** 1191
[64] Iachello F and Zamfir N V 2004 *Phys. Rev. Lett.* **92** 212501
[65] Leviatan A 2005 *Phys. Rev.* C **72** 031305(R)
[66] Leviatan A 2006 *Phys. Rev.* C **74** 051301(R)
[67] Cejnar P, Jolie J and Casten R F 2010 *Rev. Mod. Phys.* **82** 2155
[68] Iachello F 2011 *Riv. Nuovo Cimento* **34** 617
[69] Kirson M W and Leviatan A 1985 *Phys. Rev. Lett.* **55** 2846
[70] Leviatan A 1987 *Ann. Phys. (N.Y.)* **179** 201
[71] Leviatan A and Kirson M W 1990 *Ann. Phys. (N.Y.)* **201** 13
[72] Cejnar P and Jolie J 2000 *Phys. Rev.* E **61** 6237
[73] Meyer D A *et al* 2006 *Phys. Lett.* B **638** 44
[74] Van Isacker P 1983 *Phys. Rev.* C **27** 2447
[75] Jolie J, Casten R F, von Brentano P and Werner V 2001 *Phys. Rev. Lett.* **87** 162501
[76] Jolie J and Linnemann A 2003 *Phys. Rev.* C **68** 031301(R)
[77] Van Isacker P and Chen J Q 1981 *Phys. Rev.* C **24** 684
[78] Leviatan A and Shao B 1990 *Phys. Lett.* B **243** 313
[79] Ayangeakaa A D *et al* 2016 *Phys. Lett.* B **754** 254
[80] Leviatan A and Ginocchio J N 2003 *Phys. Rev. Lett.* **90** 212501
[81] Heyde K, Van Isacker P, Waroquier M and Moreau J 1984 *Phys. Rev.* C **29** 1420
[82] Zamfir N V and Casten R F 1991 *Phys. Lett.* B **260** 265
[83] Garcí a-Ramos J E, Arias J M and Van Isacker P 2000 *Phys. Rev.* C **62** 064309
[84] Bonatsos D 1988 *Phys. Lett.* B **200** 1
[85] Nomura K, Shimizu N, Vretenar D, Nikšić T and Otsuka T 2012 *Phys. Rev. Lett.* **108** 132501
[86] Hellemans V, Van Isacker P, De Baerdemacker S and Heyde K 2009 *Nucl. Phys.* A **819** 11